CHAPTER 4

Optical Nonlinearities in the Transparency Region of Bulk Semiconductors

Mansoor Sheik-Bahae

DEPARTMENT OF PHYSICS AND ASTRONOMY
UNIVERSITY OF NEW MEXICO
ALBUQUERQUE, NEW MEXICO

Eric W. Van Stryland

CENTER FOR RESEARCH AND EDUCATION IN OPTICS AND LASERS (CREOL)
UNIVERSITY OF CENTRAL FLORIDA
ORLANDO, FLORIDA

List of Abbreviations and Acronyms can be located preceding the references for this chapter.

I. Introduction

The nonlinear optical properties of semiconductors are among the first studied (Braunstein and Ockman, 1964) and continue to be extensively investigated (Haug, 1988; Miller et al., 1981a; Jain and Klein, 1983) and used for a variety of applications (e.g., optical switching (Stegeman and Wright, 1990) and short pulse production (Keller et al., 1996; Kaetner et al., 1995) (See also Vol. 59, Chap. 4). Some of the largest nonlinearities ever reported have been in semiconductors (Miller and Duncan, 1987; Hill et al., 1982) and involve near-gap excitation. However, these resonant nonlinearities, by their nature, involve significant linear absorption (see Chap. 1 in this volume and Chap. 5 in Vol. 59), which is undesirable in many applications. In this chapter we concentrate on the nonlinear response in the transparency range of semiconductors, i.e., for photon energies far enough below the bandgap energy E_g that bound-electronic nonlinearities either dominate the nonlinear response or are responsible for initiating free-carrier nonlinearities (e.g., two-photon absorption–created carrier nonlinearities). The bound-electronic nonlinearities of two-photon absorption (2PA) and the optical Kerr effect are the primary nonlinearities of interest.

The nonlinear optical behavior in the transparency region of solids due to the anharmonic response of bound valence electrons has been studied extensively in the past (Adair et al., 1987, 1989; Akhmanov et al., 1968; Flytzanis, 1975). Nonlinear refraction associated with this process is known as the *bound-electronic Kerr effect*. It is described by a change of refractive index $\Delta n = n_2 I$, where I is the light irradiance (W/cm^2) and n_2(cm^2/W) is the optical Kerr coefficient of the solid. This type of nonlinearity results from virtual intermediate transitions (Boyd, 1992) as opposed to real intermediate transitions that occur in resonant (electron-hole plasma) nonlinearities. In the language of quantum mechanics, a virtual carrier lifetime can be defined from the uncertainty principle as $1/|\omega-\omega_g|$. Here, ω is the optical frequency, and $\omega_g = E_g/\hbar$, where E_g is the band-gap energy of the solid, and $\hbar$ is Planck's constant. This equality means that in the transparency region where $\omega \ll \omega_g$, the response time is very fast ($\ll 10^{-14}$s) and can be regarded as essentially instantaneous. This ultrafast response time has been exploited in applications such as soliton propagation in glass fibers (Agrawal, 1989) and in the generation of femtosecond pulses in solid-state lasers (Kerr lens mode locking) (Spence et al., 1991). Another significant application is the development of ultrafast all-optical-switching (AOS) devices (Gibbs, 1985). Although much progress has been made in this area, development of a practical switch has been hindered by the relatively small magnitude of bound-

electronic nonlinearities. The AOS issues are discussed in more detail in Section VII.1.

The organization of this chapter is as follows: The next section (Section II) is intended to provide an elementary background in nonlinear optics and familiarize the reader with the basic definitions and relations pertaining to the ultrafast third-order nonlinear response ($\chi^{(3)}$) in materials. Section III contains a simple yet general semiclassical theory describing nonlinear absorption (NLA) and nonlinear refraction (NLR) in semiconductors. The key insight of this theory is the use of a Kramers-Kronig transformation to unite the refractive (Kerr effect) and absorptive (e.g., two-photon absorption) components of the bound-electronic nonlinearities. A simple two-parabolic-band model describes the band structure of the solid. The simplicity of this model allows for great generality, making it applicable not only to semiconductors but to large-gap optical solids as well. The results of the extension of this theory to include active semiconductors are given in Section IV. In Section V, cumulative (slow) nonlinearities due to generation of free carriers are discussed. Section VI gives a brief description of experimental techniques including Z-scan (Sheik-Bahae *et al.*, 1989, 1990b), wave-mixing schemes (Adair *et al.*, 1989), and interferometric methods (LeGasse *et al.*, 1990), while Section VII discusses a number of potential applications, namely, all-optical-switching and optical limiting. Finally, the conclusion of this chapter is presented in Section VIII.

II. Background

1.   NONLINEAR ABSORPTION AND REFRACTION

The processes of *nonlinear absorption* (NLA) and *nonlinear refraction* (NLR) in materials, in the most general case, can be considered as the interaction of two light beams having distinct frequencies (ω_a and ω_b) in a nonlinear medium. In such an interaction, the two beams can alter each other's phase (NLR) or amplitude (NLA), the latter process requiring certain energy resonances. Note that in this type of wave mixing no new frequencies are generated. The preceding condition, known as the *non-degenerate interaction*, is the general case of the simpler degenerate situation where the two beams have the same frequency ($\omega_a = \omega_b$). Most convenient experimental arrangements, however, involve an even simpler degenerate geometry where both beams have the same vector as well as frequency. In this case, which is also known as *nonlinear self-action*, a single beam alters its own phase and/or amplitude through propagation in a nonlinear medium.

In the characterization of a nonlinear material, one determines the non-linear change of refractive index (Δn) and change of absorption coefficient ($\Delta\alpha$) of a material. Relations for these changes are

$$\Delta n(\omega_a) = n_2(\omega_a; \omega_a)I_a + 2n_2(\omega_a; \omega_b)I_b \tag{1}$$

and

$$\Delta\alpha(\omega_a) = \alpha_2(\omega_a; \omega_a)I_a + 2\alpha_2(\omega_a; \omega_b)I_b \tag{2}$$

where I_b and I_b are the irradiances of the two beams. Here, n_2 and α_2 refer to the nonlinear refractive index and nonlinear absorption coefficients, respectively. For photon energies $\hbar\omega_i$ satisfying $E_g/2 < \hbar(\omega_a + \omega_b) < E_g$, α_2 accounts for 2PA and is often denoted by β. Note that without loss of generality, we assume that the measurement is performed on beam 1, while beam 2 acts as an excitation source only. The first terms on the right-hand side of the preceding equations correspond to self-action (i.e., single-beam experiments). The second terms correspond to the case of an excite-probe experiment provided that the two beams are distinguishable either by frequency and/or wavevector. The factor of 2 in front of the second term is a consequence of this distinguishability, since a higher degree of permutation is allowed in the nonlinear interaction process (Boyd, 1992). This stronger nondegenerate response is sometimes referred to as *weak-wave retardation* (Van Stryland *et al.*, 1982). While most reported measurements and applications involve degenerate self-action processes, in the theoretical treatment presented in this chapter we will consider the more general nondegenerate case while keeping in mind that the degenerate coefficients are merely the limit of the nondegenerate ones for $\omega_a = \omega_b$. Aside from the generality argument, the reason for choosing this theoretical approach becomes more apparent when we discuss the use of Kramers-Kronig dispersion relations in relating the NLR and NLA.

The nonlinear optical interactions presented in this chapter will be treated in two separate steps. The macroscopic propagation process (i.e., Maxwell equations) will be considered independently from the microscopic interaction that concerns the various mechanisms in the nonlinear response of the system. The propagation effects will be introduced first with the assumption that the nonlinear coefficients and their frequency dependence are known. The subsequent section will dwell on the microscopic calculation of the nonlinear coefficients using a simple, semiclassical two-band theory for semiconductors.

2. NONLINEAR POLARIZATION AND THE DEFINITIONS OF NONLINEAR COEFFICIENTS

a. Third-Order Nonlinearities

As defined in most nonlinear optics texts, the total material polarization P that drives the wave equation for the electric field E is (ignoring nonlocality) (Boyd, 1992)

$$\vec{P}_i(t) = \varepsilon_0 \int_{-\infty}^{\infty} R_{ij}^{(1)}(t - t_1)\vec{E}_j(t_1)dt_1 + \varepsilon_0 \int_{-\infty}^{\infty} \int_{-\infty}^{\infty} R_{ijk}^{(2)}(t - t_1, t - t_2)$$

$$\times \vec{E}_j(t_1)\vec{E}_k(t_2)dt_1 dt_2 + \varepsilon_0 \int_{-\infty}^{\infty} \int_{-\infty}^{\infty} \int_{-\infty}^{\infty} R_{ijkl}^{(3)}(t - t_1, t - t_2, t - t_3)$$

$$\times \vec{E}_j(t_1)\vec{E}_k(t_2)\vec{E}_l(t_3)\, dt_1\, dt_2\, dt_3 + \cdots \tag{3}$$

where $R^{(n)}$ is defined as the nth-order, time-dependent response function or time-dependent susceptibility. The subscripts are polarization indices indicating, in general, the tensorial nature of the interactions. The summation over the various indices $j, k, l, \ldots$ is implied for the various tensor elements of $R^{(n)}$. Ignoring the second-order effects [i.e., the second term on the RHS of Eq. (3)] corresponding to wave mixing and electro-optic processes in noncentrosymmetric materials, we focus our attention on the third-order nonlinearities. The third-order response is the first term that can directly lead to NLA or NLR. Upon Fourier transformation, we obtain

$$\vec{P}_i(\omega) = \varepsilon_0 \int_{\infty}^{-\infty} d\omega_1 \chi_{ij}^{(1)}(\omega_1)\vec{E}_j(\omega_1)\delta(\omega - \omega_1) + \varepsilon_0 \int_{\infty}^{-\infty} d\omega_1 \int_{\infty}^{-\infty} d\omega_2$$

$$\times \int_{\infty}^{-\infty} d\omega_3 \chi_{ijkl}^{(3)}(\omega_1, \omega_2, \omega_3)\vec{E}_j(\omega_1)\vec{E}_k(\omega_2)\vec{E}_l(\omega_3)$$

$$\times \delta(\omega - \omega_1 - \omega_2 - \omega_3) \tag{4}$$

where δ is the Dirac delta function. Here the nth-order susceptibility is defined as the Fourier transform of the nth-order response function:

$$\chi_{ijk\ldots n}^{(n)}(\omega_1, \omega_2, \ldots, \omega_n) = \int_{-\infty}^{+\infty} d\tau_1 \int_{-\infty}^{+\infty} d\tau_2 \cdots \int_{-\infty}^{+\infty} d\tau_n R_{ijk\ldots n}^{(n)}$$

$$\times (\tau_1, \tau_2, \ldots \tau_n)e^{i(\omega_1\tau_1 + \omega_2\tau_2 + \cdots + \omega_n\tau_n)} \tag{5}$$

For simplicity, we drop the polarization indices $i, j, \ldots$ and thus ignore the tensorial properties of $\chi^{(n)}$ as well as the vectorial nature of the electric fields at this time. The polarization effects will be discussed briefly in Sections III.3 and VI.7.

Assuming monochromatic fields, we take the general case involving the interaction of two distinct frequencies ω_a and ω_b as

$$E = \frac{E_a}{2} e^{i\omega_a t} + \frac{E_b}{2} e^{i\omega_b t} + c.c. \tag{6}$$

whose Fourier transform is

$$E(\omega) = \frac{1}{2} [E_a \delta(\omega - \omega_a) + E_a^* \delta(\omega + \omega_a) + E_b \delta(\omega - \omega_b) + E_b^* \delta(\omega + \omega_b)] \tag{7}$$

Upon substituting this into Eq. (4) and separating only the polarization terms occurring at ω_a, we obtain

$$P(\omega_a) = \varepsilon_0 \left\{ \frac{1}{2} \chi^{(1)}(\omega_a) E_a + \frac{3}{8} \chi^{(3)}(\omega_a, \omega_a, -\omega_a) E_a^2 E_a^* + \frac{6}{8} \chi^{(3)}(\omega_a, \omega_b, -\omega_b) \right.$$
$$\left. \times E_a E_b E_b^* \right\} \delta(\omega - \omega_a) + \{c.c.\} \delta(\omega + \omega_a) \tag{8}$$

Examination of Eq. (8) indicates that we can introduce an effective susceptibility χ_{eff} defined as

$$\chi_{\text{eff}}(\omega_a) = \chi^{(1)}(\omega_a) + \frac{3}{4} \chi^{(3)}(\omega_a, \omega_a, -\omega_a) |E_a|^2 + \frac{6}{4} \chi^{(3)}(\omega_a, \omega_b, -\omega_b) |E_b|^2 \tag{9}$$

where $P = \{\varepsilon_0 \chi_{\text{eff}} E_a / 2\} \delta(\omega - \omega_a) + \{c.c.\} \delta(\omega + \omega_a)$. Deriving the coefficients of nonlinear absorption and refraction from Eq. (9) is now straightforward. The complex refractive index is defined as

$$n + i\kappa = (1 + \chi_{\text{eff}})^{1/2} \tag{10}$$

Assuming that the nonlinear terms in Eq. (9) are small compared with the

linear term, we can expand Eq. (10) to obtain

$$n + i\kappa = n_0(\omega_a) + i\kappa_0(\omega_a) + \frac{3}{8n_0(\omega_a)}\chi^{(3)}(\omega_a, \omega_a, -\omega_a)|E_a|^2$$

$$+ \frac{6}{8n_0(\omega_a)}\chi^{(3)}(\omega_a, \omega_b, -\omega_b)|E_b|^2$$

$$= n_0 + i\frac{c}{2\omega_d}\alpha_0 + \Delta n + i\frac{c}{2\omega_a}\Delta\alpha \qquad (11)$$

where $n_0 = (1 + \mathcal{R}e\{\chi^{(1)}\})^{1/2}$, and it is assumed that we are operating in the transparency regime where the background linear absorption coefficient is small, $\alpha_0 \propto \mathcal{I}m\{\chi^{(1)}\} \ll \mathcal{R}e\{\chi^{(1)}\}$. The presence of a nonzero α_0 in the transparency region may be due to processes such as band tailing, lattice absorption, and free carrier absorption. We can now arrive at Eq. (1) from Eq. (11) by using the irradiance $I_i = \frac{1}{2}c\varepsilon_0 n_0(\omega_i)|E_i|^2$ ($i = a, b$) and defining

$$n_2(\omega_a; \omega_b) = \frac{3}{4\varepsilon_0 n_0(\omega_a)n_0(\omega_b)c}\mathcal{R}e\{\chi^{(3)}(\omega_a, -\omega_b, \omega_b)\} \qquad (12)$$

and

$$\alpha_2(\omega_a; \omega_b) = \frac{3\omega_a}{2\varepsilon_0 n_0(\omega_a)n_0(\omega_b)c^2}\mathcal{I}m\{\chi^{(3)}(\omega_a, -\omega_b, \omega_b)\} \qquad (13)$$

The propagation through the nonlinear medium, ignoring the effect of diffraction and dispersion (i.e., pulse distortion) inside the nonlinear material, will be governed by the following equations describing the irradiance and phase of the probe beam:

$$\frac{dI_a}{dz} = -\alpha_0(\omega_a) - a_2(\omega_a; \omega_a)I_a^2 - 2\alpha_2(\omega_a; \omega_b)I_a I_b \qquad (14)$$

and

$$\frac{d\phi_a}{dz} = \frac{\omega_a}{c}[n_0(\omega_a) + n_2(\omega_a; \omega_a)I_a + 2n_2(\omega_a; \omega_b)I_b] \qquad (15)$$

In the literature, n_2 is often used to describe the nonlinear index change due to many possible mechanisms ranging from thermal and molecular orientational to saturation of absorption and ultrafast $\chi^{(3)}$ nonlinearities. Here we restrict the use of n_2 to describe only the latter, i.e., the ultrafast bound-electronic nonlinear refraction.

Another commonly used coefficient for describing the nonlinear index is $\tilde{n}_2$, defined as

$$n = n_0 + \tilde{n}_2(\omega_a; \omega_a)\frac{|E_a|^2}{2} + 2\tilde{n}_2(\omega_a; \omega_b)\frac{|E_b|^2}{2} \tag{16}$$

where $\tilde{n}_2$ is usually given in Gaussian units (esu) and is related to n_2 through

$$\tilde{n}_2(\text{esu}) = \frac{cn}{40\pi}n_2(\text{SI}) \tag{17}$$

where the right-hand side is all in mks units (SI). However, the reader must be made aware that in the literature various symbols and definitions different from those given here may be used to describe the nonlinear refractive index. Similarly for nonlinear absorption β is often used for α_2 when describing 2PA. The various mechanisms contributing to NLA processes, including 2PA, will be discussed in Section III.

Another important piece of information contained in this pair of equations (Eqs. 12 and 13) is that since it is known that the real and imaginary parts of the linear susceptibilities are connected through causality by Kramers-Kronig relations, we expect that there should be an analogous connection between the real and imaginary parts of the nonlinear susceptibility. We discuss these relations and the associated physics next.

b. Kramers-Kronig Relations

The complex response function of any linear causal system obeys a dispersion relation that relates the real and imaginary parts via Hilbert transform pairs. In optics, these are known as *Kramers-Kronig (KK) dispersion relations* that relate the frequency-dependent refractive index $n(\omega)$ to an integral over all frequencies of the absorption coefficient $\alpha(\omega)$, and vice versa, that is,

$$n(\omega) - 1 = \frac{c}{\pi}\mathscr{P}\int_0^\infty \frac{\alpha(\omega')}{\omega'^2 - \omega^2}d\omega' \tag{18}$$

where $\mathscr{P}$ denotes the Cauchy principal value. We drop the $\mathscr{P}$ notation in what follows for simplicity, although it is always implied. An interesting way of viewing these dispersion relations was given by Toll (1956), as shown in Fig. 1(a). A wave train (a), consisting of a superimposition of many frequencies, arrives at an absorbing medium. If one frequency component
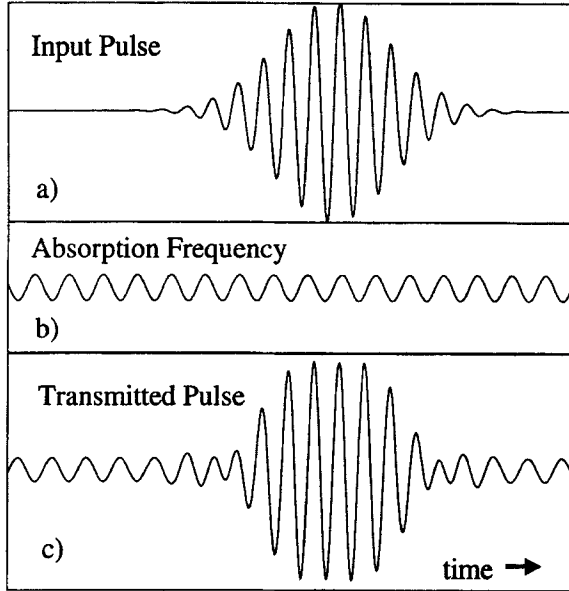
FIG. 1. Pictorial representation of the need for a relation between index and loss: (a) input pulse electric field in time; (b) absorption component in time. (c) (a) — (b). After Toll (1956).

(b) is completely absorbed, we could naively expect that the output should be given by the difference between (a) and (b), as shown in (c). However, it can be seen that such an output would violate causality with an output signal occurring at times before the incident wave train arrives. In order for causality to be satisfied, the absorption of one frequency component must be accompanied by phase shifts of all the remaining components in just such a fashion that when the components are summed, zero output results for times before the arrival of the wave train. Such phase shifts result from the index of refraction and its dispersion. The KK relation is the mathematical expression of causality. We will start with a simple derivation of the linear KK relations and then proceed to obtain similar relations pertaining to nonlinear optics.

Linear Kramers-Kronig relations. In a dielectric medium, the linear optical polarization $P(t)$ can be obtained from Eq. (3) as

$$P(t) = \varepsilon_0 \int_{-\infty}^{\infty} R^{(1)}(t)E(t - \tau)\,d\tau \tag{19}$$

The response function $R^{(1)}(\tau)$ is equivalent to a Green's function, since it gives the response (polarization) resulting from a delta-function input (electric field). In the Fourier domain, as given in Eq. (4), we have

$$P(\omega) = \varepsilon_0 \chi^{(1)}(\omega)E(\omega) \tag{20}$$

where $\chi^{(1)}(\omega)$ is the susceptibility defined in terms of the response function as

$$\chi^{(1)}(\omega) = \int_{-\infty}^{\infty} R^{(1)}(\tau)e^{-i\omega t}\, d\tau \tag{21}$$

[Note that $\chi^{(1)}(\omega)$ and $R^{(1)}(\tau)$ are not an exact Fourier transform pair because of a missing 2π.] Causality states that the effect cannot precede the cause. In the preceding case this requires that $\vec{E}(t - \tau)$ cannot contribute to $\vec{P}(t)$ for $t < (t - \tau)$. Therefore, in order to satisfy causality, $R^{(1)}(\tau) = 0$ for $\tau < 0$. An easy way to see this is to consider the response to a delta-function $E(\tau) = E_0\delta(\tau)$, where the polarization would follow $R^{(1)}(t)$. This has important consequences for the relation between the susceptiblity $\chi^{(1)}(\omega)$ and the response function $R^{(1)}(t)$, since the integration needs to be performed only for positive times. Therefore, the lower limit in the integral in Eq. (21) can in general be replaced by zero.

The usual method for deriving the KK relation from this point is to consider a Cauchy integral in the complex frequency plane. However, in the Cauchy integral method, the physical principle from which dispersion relations results (namely, causality) is not obvious. The principle of causality can be restated mathematically as

$$R^{(1)}(t) = R^{(1)}(t)\Theta(t) \tag{22}$$

i.e., the response to an impulse at $t = 0$ must be zero for $t < 0$. Here, $\Theta(t)$ is the Heaviside step function, defined as $\Theta(t) = 1$ for $t > 0$ and $\Theta(t) = 0$ for $t < 0$. [It is also possible to use the "sign" function at this point or any other function that requires $R^{(1)}(t) = 0$ for $t < 0$.] Upon Fourier transforming this equation, the product in the time domain becomes a convolution in frequency space:

$$\chi^{(1)}(\omega) = \chi^{(1)}(\omega) * \left[\frac{\delta(\omega)}{2} + \frac{i}{2\pi\omega}\right] = \frac{\chi^{(1)}(\omega)}{2} + \frac{1}{2\pi}\int_{-\infty}^{\infty}\frac{\chi^{(1)}(\omega')}{\omega - \omega'}\, d\omega'$$

$$= \frac{1}{i\pi}\int_{-\infty}^{\infty}\frac{\chi^{(1)}(\omega')}{\omega' - \omega}\, d\omega' \tag{23}$$

which is the KK relation for the linear optical susceptibility. Thus the KK relation is simply a restatement of the causality condition (Eq. 22) in the frequency domain. Taking the real part, we have

$$\mathscr{R}e\{\chi^{(1)}(\omega)\} = \frac{1}{\pi} \int_{-\infty}^{\infty} \frac{\mathscr{I}m\{\chi^{(1)}(\omega')\}}{\omega' - \omega} d\omega' \tag{24}$$

It is more standard to write the optical dispersion relations in terms of the more familiar quantities of refractive index $n(\omega)$ and absorption coefficient $\alpha(\omega)$ (Price, 1964). These relations are derived in Hutchings *et al.* (1992) using relativistic arguments. However, if we assume dilute media with small absorption and indices, we obtain the identical result. By setting $n - 1 = \mathscr{R}e\{\chi^{(1)}\}/2$ and $\alpha = \omega\mathscr{I}m\{\chi^{(1)}\}/c$, we obtain

$$n(\omega) - 1 = \frac{c}{2\pi} \int_{-\infty}^{\infty} \frac{\alpha(\omega')}{\omega' - \omega} \frac{d\omega'}{\omega'} \tag{25}$$

Since $E(t)$ and $P(t)$ are real, $n(-\omega) = n(\omega)$ and $\alpha(-\omega) = \alpha(\omega)$, which allows the integral in Eq. (25) to be written with limits from 0 to ∞ giving the final result of Eq. (18). More rigorous derivation of Eq. (25) has been given by Toll (1956) and Nussenzweig (1972).

Nonlinear Kramers-Kronig relations. Although dispersion relations for linear optics (i.e., KK relations) are well understood, confusion has existed about their application to nonlinear optics. Clearly, causality holds for nonlinear as well as linear systems. The question is: What form do the resulting dispersion relations take? The usual Kramers-Kronig relations are derived from linear dispersion theory, so it would appear impossible to apply the same logic to a nonlinear system (Hutchings *et al.*, 1992). Since the birth of nonlinear optics, there have been numerous articles addressing the dispersion relations (Kogan, 1963; Caspers, 1964; Ridener and Goud, 1975; Bassani and Scandolo, 1991). However, the usefulness of these relations was not fully appreciated and used until recently (Sheik-Bahae *et al.*, 1990a, 1991).

The simplest way to view this process is to linearize the problem. By viewing the material plus strong perturbing light beam as a new linear system on which we apply causality; we obtain a new absorption spectrum for the material, as illustrated in Fig. 2.

The linear Kramers-Kronig relation can be applied both in the presence and in the absence of a perturbation and the difference taken between the two cases. This is to say that the system remains causal under an external
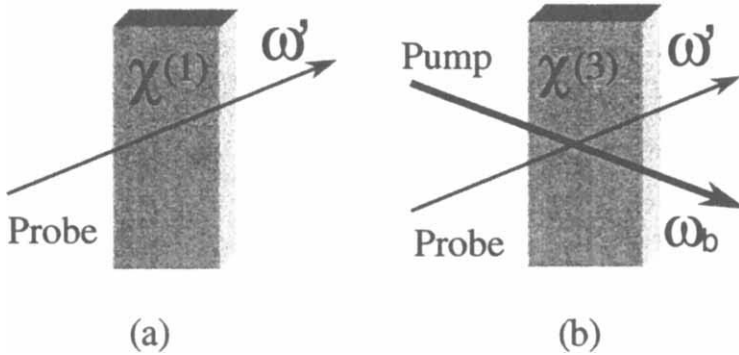
FIG. 2. (a) Linear system, material only, probed at ω' to determine the linear absorption spectrum. (b) The system is now the material plus strong light beam at ω_b, probed at ω', to determine the changed "linear" absorption spectrum.

perturbation. We can write down a modified form of the Kramers-Kronig relation (which we also derive below specifically for an optical perturbation):

$$[n(\omega) + \Delta n(\omega; \zeta)] - 1 = \frac{c}{\pi} \int_{-\infty}^{\infty} \frac{\alpha(\omega') + \Delta\alpha(\omega'; \zeta)}{\omega'^2 - \omega^2} d\omega' \qquad (26)$$

which after subtracting the linear relation between n and α leaves a relation between the changes in index and absorption:

$$\Delta n(\omega; \zeta) = \frac{c}{\pi} \int_{-\infty}^{\infty} \frac{\Delta\alpha(\omega'; \zeta)}{\omega'^2 - \omega^2} d\omega' \qquad (27)$$

where ζ denotes the perturbation. An equivalent relation also exists whereby the change in absorption coefficient can be calculated from the change in the refractive index, but this is rarely used for the reason described below. Note that it is essential that the perturbation be independent of frequency of observation ω' in the integral (i.e., the excitation ζ must be held constant as ω' is varied). This form of calculation of the refractive index for nonlinear optics is often more useful than the analogous linear optics relation. Absorption changes (which can be either calculated or measured) usually occur only over a limited frequency range, and thus the integral in Eq. (27) needs to be calculated only over this finite frequency range. In comparison, for the linear Kramers-Kronig calculation, absorption spectra tend to cover

a very large frequency range, and it is necessary to take account of this full range in order to obtain a quantitative fit for the dispersion. Unfortunately, the converse is not true, since refractive index changes are usually quite extensive in frequency.

Equation (27) has been used frequently to determine refractive changes due to "real" excitations such as thermal and free-carrier nonlinearities in semiconductors (Haug, 1988; Miller et al., 1981a; Jain and Klein, 1983). In those cases, ζ denotes either ΔT (change in temperature) or ΔN (change in free-carrier density), respectively. For example, this method has been used to calculate the refractive index change resulting from an excited electron-hole plasma (Miller et al., 1981b) and a thermal shift of the band edge (Wherrett et al., 1988). For cases where an electron-hole plasma is injected, the subsequent change in absorption gives the plasma contribution to the refractive index. In this case, the ζ parameter in Eq. (27) is taken as the change in plasma density regardless of the mechanism of generation of the plasma or the pump frequency. Van Vechten and Aspnes (1969) obtained the low-frequency limit of n_2 from a similar KK transformation of the Franz-Keldysh electro-absorption effect. In this case, ζ is the dc electric field.

Here we apply this formalism to the case where the perturbation is "virtual," occurring at an excitation frequency ω_b. To the lowest order in the excitation irradiance I_b, we write

$$\Delta\alpha(\omega_a; \zeta) = \Delta\alpha(\omega_a; \omega_b) = 2\alpha_2(\omega_a; \omega_b)I_b \quad \text{and}$$

$$\Delta n(\omega_a; \zeta) = \Delta n(\omega_a; \omega_b) = 2n_2(\omega_a; \omega_b)I_b \quad (28)$$

This leads to dispersion relations between α_2 and n_2:

$$n_2(\omega_a; \omega_b) = \frac{c}{\pi} \int_0^\infty \frac{\alpha_2(\omega'; \omega_b)}{\omega'^2 - \omega_a^2} d\omega' \quad (29)$$

We note here that even when the degenerate $n_2 = n_2(\omega_a; \omega_a)$ is desired for a given ω_a, the dispersion relations require that we should know the nondegenerate absorption spectrum $\alpha_2(\omega'; \omega_b)$ at all frequencies ω'. Also, the implication of Eq. (29) for the nonlinear susceptibility, on using Eqs. (12) and (13), is

$$\mathcal{R}e\{\chi^{(3)}(\omega_a, \omega_b, -\omega_b)\} = \frac{2}{\pi} \int_0^\infty \frac{\omega'\mathcal{I}m\{\chi^{(3)}(\omega', \omega_b, \omega_b)\}}{\omega'^2 - \omega_a^2} d\omega' \quad (30)$$

which, using the symmetry properties of $\chi^{(3)}$, also can be written as

$$\mathscr{R}e\{\chi^{(3)}(\omega_a, \omega_b, -\omega_b)\} = \frac{1}{\pi} \int_{-\infty}^{\infty} \frac{\mathscr{I}m\{\chi^{(3)}(\omega', \omega_b, \omega_b)\}}{\omega' - \omega_b} d\omega' \qquad (31)$$

Another way of deriving Eq. (31) in a more general form is by applying the causality condition directly to the nonlinear response R^n. Starting with Eq. (5), causality implies that the nonlinear susceptibility can be determined by integration over positive times only:

$$\chi^{(n)}(\omega_1, \omega_2, \ldots, \omega_n) = \int_0^{\infty} d\tau_1 \cdots \int_0^{\infty} d\tau_n R^{(n)}(\tau_1, \tau_2, \ldots, \tau_n)$$
$$\times \exp[-i(\omega_1\tau_1 + \omega_2\tau_2 + \cdots + \omega_n\tau_n)] \qquad (32)$$

It is now possible to apply the method used earlier for the linear susceptibility in order to derive a dispersion relation for the nonlinear susceptibility. For example, we can write

$$\chi^{(n)}(\tau_1, \tau_2, \ldots, \tau_n) = \chi^{(n)}(\tau_1, \tau_2, \ldots, \tau_n)\Theta(\tau_j) \qquad (33)$$

and then calculate the Fourier transform of this equation. Here j can apply to any one of the indices $1, 2, \ldots, n$. We also could use any number and combination of step functions; however, the simplest result is obtained by taking just one.

Following the same procedure as for a linear response, we obtain

$$\chi^{(n)}(\omega_1, \omega_2, \ldots, \omega_n) = \frac{-i}{\pi} \int_{-\infty}^{\infty} \frac{\chi^{(n)}(\omega_1, \omega_2, \ldots, \omega', \ldots, \omega_n)}{\omega_j - \omega'} d\omega' \qquad (34)$$

where, by equating the real and imaginary parts on both sides, we get the generalized Kramers-Kronig relation for a nondegenerate nonlinear susceptibility:

$$\mathscr{R}e\{\chi^{(n)}(\omega_1, \omega_2, \ldots, \omega_n)\} = \frac{1}{\pi} \int_{-\infty}^{\infty} \frac{\mathscr{I}m\{\chi^{(n)}(\omega_1, \omega_2, \ldots, \omega', \ldots, \omega_n)\}}{\omega' - \omega_j} d\omega'$$
$$(35)$$

In particular, for $\chi^{(3)}$ processes having $\omega_1 = \omega_a$, $\omega_2 = \omega_b$, and $\omega_3 = -\omega_b$, this becomes identical to Eq. (31) derived earlier. When including harmonic-

generating susceptibilies, however, Eq. (35) can be further generalized as given in Hutchins *et al.,* (1992).

The key concept described by Eq. (29) is that once we calculate the change in absorption spectrum induced by an excitation at ω_b, the nonlinear refraction n_2 can be obtained by performing the KK dispersion integration. We emphasize again that even degenerate $n_2(\omega_a = \omega_b)$ must be derived from a nondegenerate nonlinear absorption spectrum. In the following section, the calculation of $\alpha_2(\omega_a; \omega_b)$ [equivalently $\Delta\alpha(\omega_a; \omega_b)$] using a two-parabolic-band (TPB) model for semiconductors is described.

III. Theory of Bound-Electronic Nonlinearities: Two-Band Model

1. NONDEGENERATE NONLINEAR ABSORPTION

In this section we calculate the nonlinear absorption originating from $\chi^{(3)}$ by including 2-photon absorption (2PA), the AC Stark effect, and Raman contributions (Sheik-Bahae *et al.,* 1991, 1994). Widely available experimental results for degenerate 2PA serve as a calibration for the calculation. Analysis of 2PA processes requires that perturbation theory be taken to second order (Worlock, 1972). A variation of this is to use first-order perturbation theory with a "dressed" initial and final state where the effect of the acceleration of the electrons due to the oscillating electric field is already taken into account. We use the dipole approximation for the radiation interaction Hamiltonian:

$$H_{int} = -\frac{e}{m_0}\vec{A}\cdot\vec{p} \tag{36}$$

where $\vec{A}$ is the vector potential, $\vec{p}$ is the momentum operator, $-e$ is the electronic charge, and m_0 is the bare electron mass. We assume a two-beam interaction with both beams linearly polarized in the same direction. This last assumption allows us to write the following simple expression for $\vec{A}$:

$$\vec{A} = \vec{a}_1 A_{01}\cos(\omega_1 t) + \vec{a}_2 A_{02}\cos(\omega_2 t) \tag{37}$$

where A_{01} and A_{02} are the vector field amplitudes at frequencies ω_1 and ω_2, respectively (Note: In this section we use ω_1 and ω_2 instead of ω_a and ω_b.) $\vec{a}_1$ and $\vec{a}_2$ are the polarization unit vectors and are taken parallel for the calculations presented in this section. The case of orthogonal polarization will be discussed briefly in Section III.3. Following Keldysh (1965), Jones

and Reiss (1977), and Brandi and de Araujo (1983), the initial (valence band) and the final (conduction band) states can be approximated by Valkov-type wavefunctions (Volkov, 1935):

$$\psi_{c,v}(\vec{k}, \vec{r}, t) = u_{c,v}(\vec{k}, \vec{r}) \exp\left[i\vec{k} \cdot \vec{r} - \frac{i}{\hbar} \int_0^t E_{c,v}(\tau) \, d\tau \right] \tag{38}$$

where $u_{c,v}(\vec{k} \cdot \vec{r})$ is the usual Bloch wavefunction for the conduction (c) or valence (v) band states, and the corresponding AC (or optical) Stark-shifted energy of the states are given by

$$E_{c,v} = E_{c,v}^0 + \Delta E_{c,v}^{(1)}(\tau) + \Delta E_{cv}^{(2)} \tag{39}$$

Within the effective mass approximation and using the two-parabolic-band (TPB) model, the unperturbed energies of the final and ground states are given by

$$E_c^0 = E_g + \frac{\hbar^2 k^2}{2m_c} \tag{40a}$$

and

$$E_v^0 = \frac{\hbar^2 k^2}{2m_v} \tag{40b}$$

where k is an electron wavevector, and m_c and m_v are the conduction and valence band effective masses, respectively. The linear optical Stark shift of the energy bands is given by

$$\Delta E_{ii}(\tau) = \frac{-eh}{m_i} \vec{k} \cdot \vec{A}(\tau) \tag{41}$$

The quadratic optical Stark effect (QSE) resulting from the coupling between conduction and valence bands due to ω_2 is written as

$$\Delta E_{cv} = -\Delta E_{vc} = \left(\frac{eA_{02}}{2m_0}\right)^2 |\vec{a}_2 \cdot \vec{p}_{cv}|^2 \left(\frac{1}{E_c^0 - E_v^0 - \hbar\omega_2} + \frac{1}{E_c^0 - E_v^0 + \hbar\omega_2}\right) \tag{42}$$

where p_{cv} is the interband momentum matrix element:

$$\vec{p}_{cv} = \frac{\hbar}{i} \int d^3\vec{r} \, u_c^*(\vec{k}, \vec{r}) \nabla u_v(\vec{k}, \vec{r}) \tag{43}$$

In the TPB model using Kane's $k \cdot p$ theory, we have that

$$m_c = -m_v \approx m_0 \frac{E_g}{E_p} \tag{44}$$

where $E_p = 2|p_{cv}(k = 0)|^2/m_0 \approx 21$ eV is the Kane energy, which is essentially material-independent for most semiconductors (Kane, 1957, 1980).

The transition rates are calculated using an S matrix formalism with (Wu and Ohmura, 1962)

$$S = \frac{i}{\hbar} \int_{-\infty}^{t} dt' \int d^3\vec{r} \psi_c^*(\vec{k}, \vec{r}, t') H_{\text{int}} \psi_v(\vec{k}', \vec{r}, t') \tag{45}$$

The transition rate W is then obtained from

$$W = \lim_{t \to \infty} \int \frac{d^3\vec{k}}{(2\pi)^3} \frac{d}{dt} |S|^2 \tag{46}$$

The transition rate given by Eq. (46) is highly nonlinear and includes all N-photon transitions ($N = 1, 2,..., \infty$) involving one virtual interband transition followed by $N - 1$ self-transitions. In this analysis, we are only concerned with the $\chi^{(3)}$ processes. In the expansion of W, therefore, we retain only the terms that are proportional to $I_1 I_2$ (where $I_j = \varepsilon_0 n_j c\omega_j^2 A_{oj}^2/2$) that involve the absorption of one photon with energy $\hbar\omega_1$. This gives the change of absorption at ω_1 due to the presence of ω_2:

$$\Delta\alpha(\omega_1, \omega_2) = 2\alpha_2(\omega_1, \omega_2)I_2 = \frac{\hbar\omega_1 W}{I_1} \tag{47}$$

The physical processes emerging from this formulation are as follows. First, there is a nondegenerate 2PA that requires $\hbar\omega_1 + \hbar\omega_2 \geq E_g$. Second is an electronic Raman transition for which $|\hbar\omega_1 - \hbar\omega_2| \geq E_g$ is required. In the "dressed state" formalism, these two processes are a consequence of the first-order (time varying) AC Stark shift described by Eq. (41). In addition to the absorption of one photon at ω_1, there is simultaneous absorption (2PA) or emission (Raman) of a photon at the excitation frequency ω_2. A third process is due to a combination of linear and primarily quadratic AC Stark effects. These only affect the photon absorption at ω_1 and hence occur for $\hbar\omega_1 \geq E_g$. This process can be viewed as saturation of absorption due to state blocking caused by virtual carriers
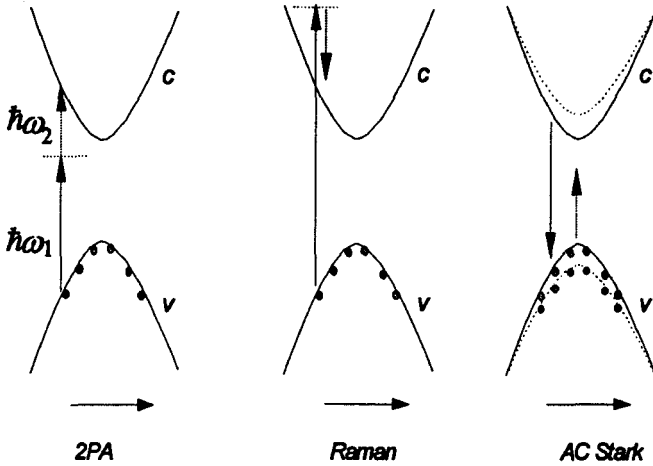
FIG. 3.   Graphic representation of the processes involved in the nonlinear absorption in a two-band model. The small circles denote bound electrons.

generated by ω_2. This effect is also referred to as *virtual band blocking*. All three processes described here are depicted graphically in Fig. 3.

The resulting representation of α_2 for 2PA has the simple form

$$\alpha_2(\omega_1, \omega_2) = K \frac{\sqrt{E_p}}{n_{01}n_{02}E_g^3} F_2(x_1, x_2) \qquad (48)$$

where K is a material-independent constant:

$$K = \frac{2^9\pi}{5} \frac{1}{(4\pi\varepsilon_0)^2} \frac{e^4}{\sqrt{m_0c^2}} \qquad (49)$$

The function F_2 involves only the parameters $x_1 = \hbar\omega_1/E_g$ and $x_2 = \hbar\omega_2/E_g$ and reflects the band structure and intermediate states considered in the calculations. In our simple model, F_2 contains contributions from 2PA, Raman, and optical Stark effects. These different components are listed in Table I, and the function F_2 is plotted in Fig. 4 for different values of x_1 and x_2.

Of the nonlinear absorption processes described here, only 2PA has been studied extensively. For over three decades, the 2PA coefficient ($\beta = \alpha_2^{(2PA)}$) has been measured for semiconductors and other optical solids. More recently, the magnitude, band-gap scaling, and spectral variation of 2PA in

TABLE I

CONTRIBUTIONS TO THE NONLINEAR ABSORPTION SPECTRAL FUNCTION $F_2(x_1, x_2)$

Contribution	$F_2(x_1, x_2)$
2-photon absorption $x_1 + x_2 > 1$	$\dfrac{(x_1 + x_2 - 1)^{3/2}}{2^7 x_1 x_2^2}\left(\dfrac{1}{x_1} + \dfrac{1}{x_2}\right)^2$
Raman $x_1 - x_2 > 1$	$\dfrac{(x_1 - x_2 - 1)^{3/2}}{2^7 x_1 x_2^2}\left(\dfrac{1}{x_1} - \dfrac{1}{x_2}\right)^2$
AC Stark $x_1 > 1$	$-\dfrac{1}{2^9 x_1 x_2^2 (x_1 - 1)^{1/2}}\left[\dfrac{x_1}{x_1^2 - x_2^2} - \dfrac{2(x_1 - 1)(x_1^2 + x_2^2)}{(x_1^2 - x_2^2)^2} + \dfrac{8(x_1 - 1)^2}{x_2^2}\right]$

semiconductors have been obtained using standard transmission measurements (Van Stryland *et al.*, 1985b). The experimental data are in good agreement with the calculation presented here. We are now in a position to look at the spectral dependence of the degenerate 2PA. From Table I the 2PA contribution to the nonlinear absorption for $x_1 = x_2 \equiv x$ is

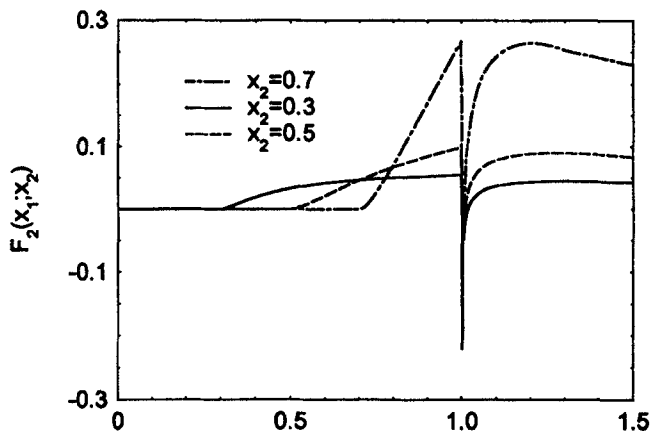$$F_2 = \frac{(2x - 1)^{3/2}}{2^5 x^5} \tag{50}$$

FIG. 4. The nonlinear absorption spectral function F_2 showing the change of absorption at ω_1 due to three different photon energies ω_2.
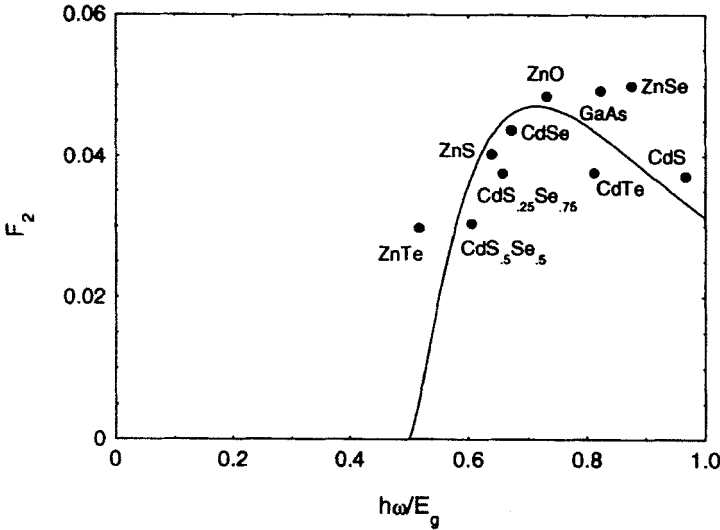
FIG. 5.   The degenerate 2PA spectral function $F_2(\hbar\omega/E_g)$ along with data scaled according to Eq. (51). (Data using transmittance from Van Stryland et al., 1985b.)

The solid line in Fig. 5 shows this spectral dependence. This functional dependence, as well as the scaling, also can be derived directly from second-order perturbation theory (Wherrett, 1984).

Comparison with experiment is done best by measuring the nonlinear absorption spectrum for individual materials. Unfortunately, there are few materials for which nonlinear spectra are known. One reason for this is that tunable sources with the required irradiance, pulse width, and beam quality are not typically available. Instead, we scale the material dependence using predictions of the two-band model [Eq. (48) with $x_1 = x_2$ and Eq. (50)]. Now experimental data for β (β^e) can be plotted by calculating the experimental value of the function F_2, F_2^e, as given below. The absolute magnitude for this function is then a fitting parameter K:

$$F_2^e(\hbar\omega/E_g) = \frac{1}{K\sqrt{E_p}}\, n_0^2 E_g^3 \beta^e \tag{51}$$

Figure 5 plots scaled data for several semiconductors versus $\hbar\omega/E_g$, with the predicted dependence from the TPB model (Van Stryland et al., 1985b). Measurements of degenerate β on a number of II-VI and III-V semiconductors fit this model using $K = 3100\,\text{cm}\,\text{GW}^{-1}\,\text{eV}^{5/2}$ in units where E_p and E_g are in electronvolts ($3.2 \times 10^{-55}\,\text{mks}$) (Van Stryland et al., 1985a). This
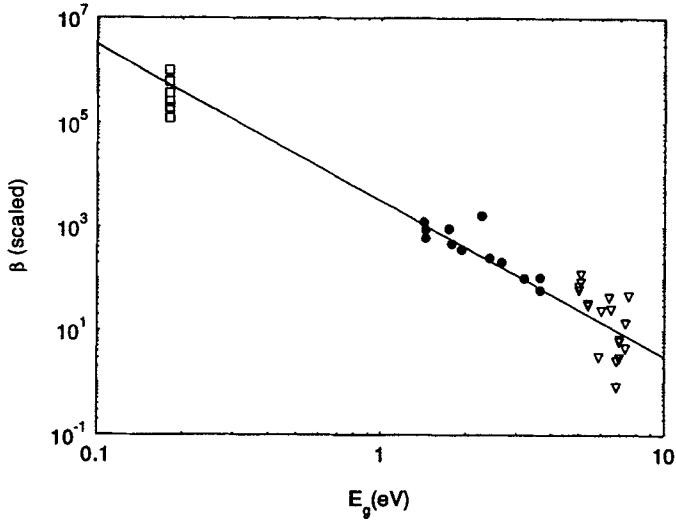
FIG. 6. Log-log plot of scaled β^* as a function of E_g. The straight line is of Eq. (51) showing the E_g^{-3} dependence. Adapted from Van Stryland *et al.* (1988).

compares favorably with the theoretical value of $K = 1940\,\mathrm{cm}\,\mathrm{GW}^{-1}\,\mathrm{eV}^{5/2}$ ($1.99 \times 10^{-55}\,\mathrm{mks}$) given by Eq. (49). We believe that the theory underestimates the empirical value because only one valence band (light-hole) has been considered, and the contribution of the heavy-hole band has been ignored. This figure shows 2PA turning on sharply at half the band-gap energy and then slowly decreasing for photon energies approaching the band gap. This behavior is similar to the behavior of linear absorption but shifted by a factor of 2 in wavelength. We will see later that the nonlinear refraction similarly mimics the linear refraction but shifted by a factor of 2 in wavelength. The E_g^{-3} dependence of 2PA is better displayed on a log-log plot scaling the data with F_2, as shown in Fig. 6. This shows that even dielectric materials follow the general trend predicted by Eq. (51). We also remark that the result derived for 2PA using first-order perturbation and dressed wavefunctions is identical to that obtained from a calculation using second-order perturbation theory (Wherrett, 1984).

2. NONDEGENERATE NONLINEAR REFRACTION

With the nondegenerate nonlinear absorption coefficient $\alpha_2(\omega_1, \omega_2)$ determined, the next step is to perform the KK transformation of Eq. (29)

to obtain the n_2 coefficient. The result of this calculation is

$$n_2(\omega_1, \omega_2) = K' \frac{\sqrt{E_p}}{n_{01}n_{02}E_g^4} G_2(x_1, x_2) \tag{52}$$

where the dispersion function G_2 is given by

$$G_2(x_1, x_2) = \frac{2}{\pi} \int_0^\infty \frac{F_2(x'; x_2)}{x'^2 - x_1^2} dx' \tag{53}$$

and

$$K' = \frac{\hbar c K}{2} = \frac{2^4}{5\pi} \frac{\hbar e^4}{\varepsilon_0^2 \sqrt{m_0} c} \tag{54}$$

Using the function F_2 given in Table I, the integration in Eq. (53) can be performed analytically. In the low-frequency limit, however, it is found that G_2 diverges as x_2 tends to zero (equivalently, $\omega_2 \to 0$). This divergence is not unexpected. The transition rate calculation is based on $A \cdot p$ perturbation theory, and it is well known that divergences of this order can be introduced. The equivalent $E \cdot r$ perturbation approach, as was shown by Aversa et al., (1994) avoids such divergences at the expense of a more intensive calculation. To examine the "infrared" divergences, the nonlinear refractive terms can be expanded in a Laurent series around $\omega_2 = 0$. Because of their unphysical nature, it has been common practice to subtract the divergent terms in the series. This brute-force process of divergence removal effectively enforces a sum rule for the two-band system. The long-wavelength divergent terms for each contribution are removed separately, and the final results are set out in Table II.

The dispersion function G_2 is depicted in Fig. 7 as a function of $x_1 = \hbar\omega_1/E_g$ for various excitation photon energies $x_2 = \hbar\omega_2/E_g$. By examining the terms in Table II individually, we can determine their relative contribution to n_2 in different spectral regimes. A general trend is evident in all the curves: n_2 is nondispersive in the infrared regime ($\hbar\omega_1 \ll E_g$), where the 2PA and Raman terms contribute almost equally. It then reaches a two-photon resonance at $\hbar\omega_1 + \hbar\omega_2 \approx E_g$, where the peak positive value is attained. Above the two-photon resonance, n_2 becomes "anomalously" dispersive and ultimately turns negative. The negative behavior of n_2 is caused primarily by the 2PA and quadratic AC Stark effect components as $\hbar\omega_1$ approaches E_g. Recent measurements of nondegenerate n_2 with the semiconductors ZnS and ZnSe, as shown in Section VI.7, show excellent agreement with this predicted behavior (Sheik-Bahae et al., 1994, 1990a).

<div align="center">TABLE II</div>

THE NONDEGENERATE DISPERSION FUNCTION FOR THE ELECTRONIC KERR COMPONENT OF n_2, CALCULATED BY A KK TRANSFORMATION OF F_2 (Table I)

Contribution	$G_2(x_1; x_2)$
2PA	$H(x_1, x_2) + H(-x_1, x_2)$
Raman	$H(x_1, -x_2) + H(-x_1, -x_2)$

where $H(x_1, x_2) = \dfrac{1}{2^6 x_1^4 x_2^4}$

$$\times \begin{bmatrix} \dfrac{5}{16}x_2^3 x_1^2 + \dfrac{9}{8}x_2^2 x_1^2 - \dfrac{9}{4}x_2 x_1^2 - \dfrac{3}{4}x_2^3 - \dfrac{1}{32}x_2^3 x_1^2(1 - x_1)^{-3/2} \\[2mm] + \dfrac{1}{2}(x_2 + x_1)^2 [(1 - x_2 - x_1)^{3/2} - (1 - x_1)^{3/2}] \\[2mm] - \dfrac{3}{16}x_2^2 x_1^2 [(1 - x_1)^{-1/2} + (1 - x_2)^{-1/2}] + \dfrac{3}{2}x_2 x_1^2(1 - x_2)^{1/2} \\[2mm] + \dfrac{3}{2}x_2^2 x_1(1 - x_1)^{1/2} + \dfrac{3}{4}x_2(x_2^2 + x_1^2)(1 - x_1)^{1/2} \\[2mm] - \dfrac{3}{8}x_2^3 x_1(1 - x_1)^{-1/2} + \dfrac{1}{2}(x_2^2 + x_1^2)[1 - (1 - x_2)^{3/2}] \end{bmatrix}$$

AC Stark

$x_1 \neq x_2$ $\quad \dfrac{1}{2^9 x_1^2 x_2^2} \begin{bmatrix} -\dfrac{1}{2} - \dfrac{4}{x_1^2} + \dfrac{4}{x_2^2} - \dfrac{x_2^2}{x_1} \dfrac{[(1 - x_1)^{-1/2} - (1 + x_1)^{-1/2}]}{x_1^2 - x_2^2} \\[2mm] + \dfrac{2x_1^2(3x_2^2 - x_1^2)}{x_2^2(x_1^2 - x_2^2)^2}[(1 - x_2)^{1/2} + (1 + x_2)^{1/2}] \\[2mm] - \dfrac{2x_2^2(3x_1^2 - x_2^2)}{x_1^2(x_1^2 - x_2^2)^2}[(1 - x_1)^{1/2} + (1 + x_1)^{1/2}] \end{bmatrix}$

$x_1 = x_2$ $\quad \dfrac{1}{2^9 x_1^4}\left[\dfrac{3}{4}\dfrac{(1 - x_1)^{-1/2} - (1 + x_1)^{-1/2}}{x_1} - \dfrac{(1 - x_1)^{-3/2} + (1 + x_1)^{-3/2}}{8} - \dfrac{1}{2}\right]$

Note: The infrared divergent terms associated with each contribution have been removed. The last term is due to the degenerate AC Stark effect, which is the limit of the nondegenerate G_2^{acStark} as $x_1 \to x_2$.

While knowledge of the dispersion of the nondegenerate n_2 may be useful for applications that employ harmonic generation crystals, for example, the major practical interest concerns the degenerate $n_2(\omega_1 = \omega_2)$. In the remainder of this chapter we focus our attention on this quantity $n_2(\omega)$. The dispersion and band-gap scaling of $n_2(\omega)$ are given by Eq. (52) with
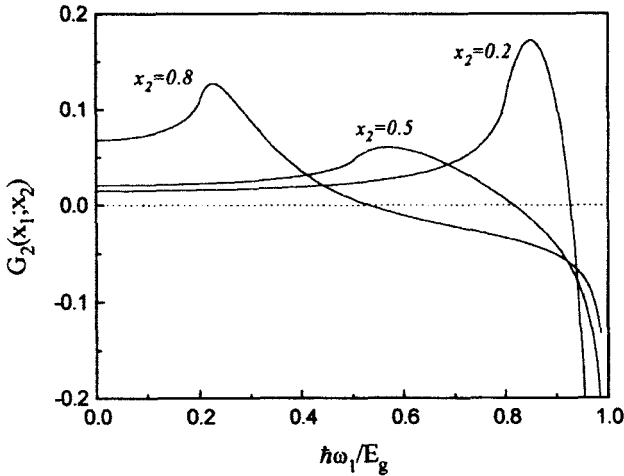
FIG. 7. The nondegenerate dispersion function $G_2(x_1, x_2)$ as a function of probe photon energy (x_1), calculated for three excitation photon energies.

$\omega_1 = \omega_2 = \omega$ and $n_{01} = n_{01} = n_0$. As was the case with the nondegenerate n_2, the two features of interest in the n_2 coefficient are the band-gap energy scaling and dispersion. The former is characterized by an E_g^{-4} scaling, while the latter exhibits a sign reversal as $\hbar\omega$ approaches E_g and also a two-photon resonance enhancement. We can now use the results of the KK integral for $G_2(\omega_1; \omega_2)$ to give the degenerate G_2 and compare with experimental data.

As for β, measuring the frequency dependence of n_2 for a single material is very difficult, and few data exist. Scaling data according to Eq. (52) (degenerate $x_1 = x_2 = x$) allows us to compare experimental measurements made on different materials. Figure 8 shows the dispersion (G_2) of n_2 as predicted by Eq. (52) along with data (n_2^e) from several experiments scaled according to Sheik-Bahae et al., (1991)

$$G_2^e(x) = \frac{n_0^2 E_g^4}{K'\sqrt{E_p}} n_2^e \tag{55}$$

It is worth mentioning that the band-gap scaling predicted by the TPB model also can be obtained using a quasi-dimensional analysis. Such an analysis was used by Wherrett to obtain the band-gap energy scaling of β. This scaling directly gives the E_g^{-4} scaling of n_2, since n_2 is directly proportional to $\chi^{(3)}$, and Wherrett (1984) showed that $\chi^{(3)} \propto E_g^{-4}$.
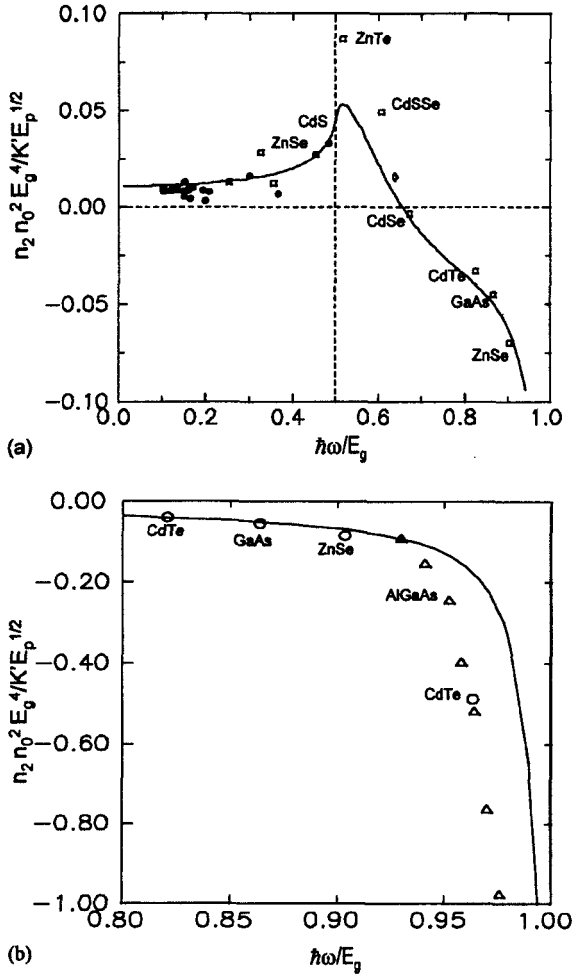
FIG. 8. A plot of experimental values of the nonlinear refractive index n_2^e scaled according to Eq. (55) versus $x = \hbar\omega/E_g$. The solid line is the two-parabolic-band-model prediction for the dispersion function G_2. (a) Circles from Adair (1989), diamond from Ross *et al.* (1990), and squares from Sheik-Bahae *et al.* (1991). (b) An extension of (a) for frequencies near the band edge (expanded scale); triangles from LaGasse *et al.* (1990). Adapted from Sheik-Bahae *et al.* (1991).

The hidden E_g^{-4} scaling can be displayed more conveniently on a log-log plot of n_2 scaled by the dispersion function G_2, as in Fig. 9. Here it is seen that the nonlinear index varies from $7.6 \times 10^{-17} \text{cm}^2/\text{W}$ for MgF_2 at $1.06\,\mu\text{m}$ to $-3.3 \times 10^{-12} \text{cm}^2/\text{W}$ for AlGaAs at 810 nm and $2.8 \times 10^{-13} \text{cm}^2/\text{W}$ for Ge at $10.6\,\mu\text{m}$. Note, for example, that although the
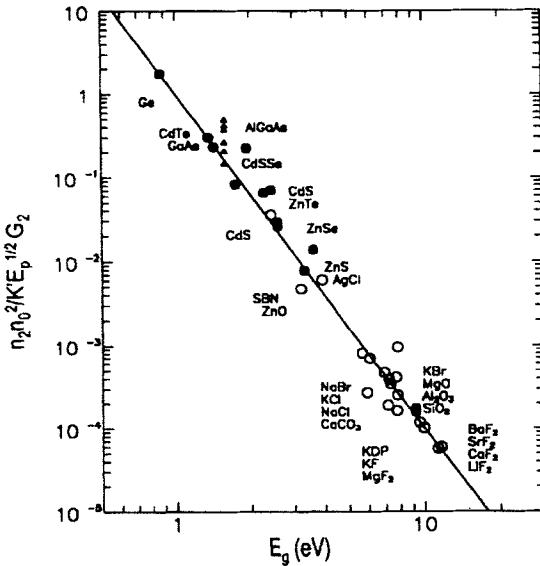
FIG. 9.   Log-log plot of scaled n_2^c as a function of E_g showing the E_g^{-4} dependence (straight line). The AlGaAs data are taken from LaGasse *et al.* (1990), and much of the large-band-gap data are from Adair *et al.* (1989). Adapted from Sheik-Bahae *et al.* (1991).

measured values of n_2 for ZnSe at 1.06 and 0.532 μm have different signs, both measurements are consistent with the scaling law.

The prefactor K', as given by Eq. (54), is 3.2×10^{-81} (mks units). If we use the K as determined by a best fit to the 2PA experimental data, we find $K' \approx 5 \times 10^{-81}$ (mks). This compares well with $K' \approx 9 \times 10^{-81}$ (mks) determined by an overall best fit to the experimental values of n_2 in semiconductors, as shown in Fig. 9. As in the 2PA case, it is more convenient to define the K' factor in mixed units such that n_2 is given by square centimeters per watt and E_p and E_g are given in electronvolts. In this case, $K' \approx 6 \times 10^{-11}$ (cm^2/W)(eV)$^{7/2}$ corresponds to the overall best fit to semiconductor n_2 data. As pointed out for the 2PA case, the factor of 2 to 3 discrepancy between theory and experiments can be attributed in part to using a single valence band (light hole) and ignoring the transition originating from the heavy-hole valence band. Moreover, as described by Sheik-Bahae *et al.* (1994), inclusion of electron-hole Coulomb interaction by multiplying the F_2 function by a generalized exciton enhancement factor will further improve the agreement between theory and experiment.

A number of theoretical efforts to extend the simple TPB model to a more compex system have been reported. For example, Hutchings and Wherrett (1994, 1995) used a Kane four-band structure to calculate the dispersion of

n_2 in zinc blende semiconductors. Aversa et al. (1994), as mentioned earlier, used $E \cdot r$ instead of $A \cdot p$ perturbation to calculate n_2 in order to avoid the unphysical infrared divergences. Interestingly, the resulting dispersion, magnitude, and scaling properties of the preceding theories are nearly identical to the simple TPB theory presented here.

Efforts also have been made to extend the n_2 theory to include quantum-confined structures. Khurgin (1994) calculated n_2 for quantum well and quantum wire structures by applying the KK transformation to the calculated two-photon absorption spectrum. Cotter et al. (1992) also calculated n_2 in quantum-confined semiconductor nanocrystals. They obtained a dispersion function that is similar to bulk materials but changes sign (i.e., becomes negative) at longer wavelengths due to an enhanced quadratic Stark effect.

3. POLARIZATION DEPENDENCE AND ANISOTROPY OF $\chi^{(3)}$

The anisotropy of the band structure, reflecting the crystalline structure of a particular semiconductor, manifests itself in the NLO properties by making n_2 and α_2 (or β) anisotropic as well. A number of theoretical considerations as well as experimental measurements have been reported dealing primarily with the anisotropy of two-photon absorption in semiconductors belonging to various symmetry groups (Rader and Gold, 1968; Dvorak et al., 1994; De Salvo et al., 1993; Balterameyunas et al., 1982).

Even in an isotropic material, such as polycrystalline semiconductors, the effect of the polarization of the incident electric field can still be studied by conducting induced-anisotropy experiments. Such experiments include polarization-dependent four-wave mixing, excite probe, and measurements of linear/circular dichroism. A simple extension of the TPB model of Section III, including the effect of the heavy-hole (hh) valence band, can provide the necessary insight into the observed polarization effects (Sheik-Bahae et al., 1995). The basic principle behind this theory lies in the k-space orientation of the momentum matrix element $\vec{p}_{cv}$ with respect to the lattice wave vector $\vec{k}$. Within Kane's $k \cdot p$ formalism (Kane, 1980), $\vec{k} \| \vec{p}_{cv}$ for the light-hole-to-conduction-band (lh-c) transitions (as used in Section III.1), while $\vec{k} \perp \vec{p}_{cv}$ for the hh-c transitions. The latter orientation can be interpreted as the reason for the bare electron effective mass (m_0) of the hh band because $k \cdot p$ coupling between that band and the conduction band vanishes. The significance of this k-space symmetry becomes apparent if we examine the expression for the transition rate due to the Raman effect and 2PA as obtained from Eq. (46):

$$W_{\vec{k}}^{2PA+Raman} \propto \int \left| \frac{(\vec{a}_1 \cdot \vec{p}_{cv})(\vec{a}_2 \cdot \vec{k})}{\omega_1} \pm \frac{(\vec{a}_2 \cdot \vec{p}_{cv})(\vec{a}_1 \cdot \vec{k})}{\omega_2} \right|^2 \delta(\hbar\omega_1 \pm \hbar\omega_2 - E_{cv}) \, d\vec{k}$$

(56)

where unit vectors $\vec{a}_1$ and $\vec{a}_2$ represent the polarization of the two optical fields at frequency ω_1 and ω_2, respectively. The sequence of transitions in Eq. (56) is typical of a two-band case in which a photon is absorbed in an interband transition followed by an absorption ($+$ sign) or emission ($-$ sign) of the second photon in an intraband process (self-transition). Using the k-space orientation properties of $\vec{k}$ and $\vec{p}_{cv}$, as discussed earlier, Eq. (56) leads to distinctly different polarization dependences for the two band pairs. For example, for the $hh\text{-}c$ system, the following relationship for the degenerate $\mathcal{I}m\{\chi^{(3)}\}$ is derived:

$$\chi_{1212} = \chi_{1221} = \frac{3}{4}\chi_{1111} \quad \text{and} \quad \chi_{1122} = -\frac{1}{2}\chi_{1111} \qquad (57)$$

whereas the $lh\text{-}c$ system follows the $\chi_{1122} = \chi_{1212} = \chi_{1221} = \chi_{1111}/3$ symmetry. In contrast, the nondegenerate transition rate due to the QSE involves only interband transitions:

$$W_{\vec{k}}^{QSE} \propto \int |(\vec{a}_1 \cdot \vec{p}_{cv})(\vec{a}_2 \cdot \vec{p}_{cv})|^2 \delta(\hbar\omega_1 - E_{cv}) d\vec{k} \qquad (58)$$

The lack of self-transitions makes the symmetry relations for χ^{QSE} the same ($\chi_{1122} = \chi_{1212} = \chi_{1221} = \chi_{1111}/3$) for both band pairs. In adding up all the contributions of the two-band pairs for both refractive and absorptive processes, one obtains the dispersion of the $\chi^{(3)}$ tensor for an isotropic three-band system. The result of this calculation can explain the observed polarization dependence in four-wave mixing and Z-scan experiments (Sheik-Bahae et $al.$, 1995). Figure 10 shows the calculated dispersion of circular/linear dichroism [defined as the ratio of n_2 (circular pol.) to n_2 (linear pol.)] as compared with experimental results obtained with some semiconductors as well as dielectrics. Similar dispersion of the dichroism also was derived by Hutchings and Wherrett (1994) using a Kane four-band model.

IV. Bound-Electronic Optical Nonlinearities in Active Semiconductors

The ultrafast NLA and NLR in semiconductor laser amplifier (SLA) waveguides have been the subject of recent studies using femtosecond self-phase modulation and pump-probe techniques (see Volume 59, Chap. 2)(Hultgren and Ippen, 1991; Hultgren et $al.$, 1992; Hall et $al.$, 1993; Fisher
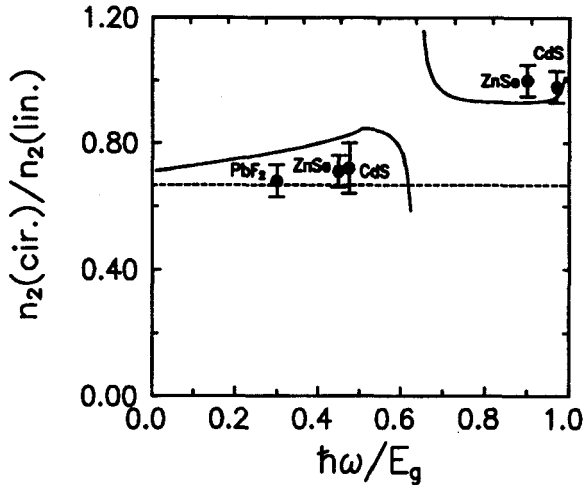
FIG. 10. The dispersion of the polarization dichroism of n_2 measured using Z-scan. The solid line is from the three-band theory, and the dashed line represents the two-band model. The divergence near $\hbar\omega/E \cong 0.65$ corresponds to the zero crossing of n_2 (linear polarization) at that wavelength. Figure from Sheik-Bahae et al. (1991).

et al., 1993; Hong et al., 1994; Grant and Sibbet, 1991). These delicate measurements revealed some intriguing features, including large, near-instantaneous, bound-electronic nonlinear refraction as well as transient carrier effects. The fast, bound-electronic nonlinearity, coupled with the low loss associated with the SLA, makes this device very attractive for possible use in all-optical interchange applications. The SLA exploits ultrafast nonlinear refraction without suffering concomitant absorption that plagues the approaches based on passive materials.

Since in this chapter our interest lies in the ultrafast n_2, we are not immediately concerned with long-lived processes that result from net carier excitation or deexcitation. As discussed in Volume 59, Chapter 2, in practice, operating at the transparency point of the device, adjusting the wavelength, and/or controlling the injected current density of the SLA can turn off such processes. However, even at the transparency point ($\hbar\omega = E_g$), there exist real excitation processes that accompany the bound-electronic component. These processes include spectral hole burning (SHB) and free-carrier absorption, both of which lead to carrier heating that shifts the transparency point.

Here we briefly discuss the results of the theory of bound-electronic n_2 in active semiconductors (Sheik-Bahae and Van Stryland, 1994). This formal-
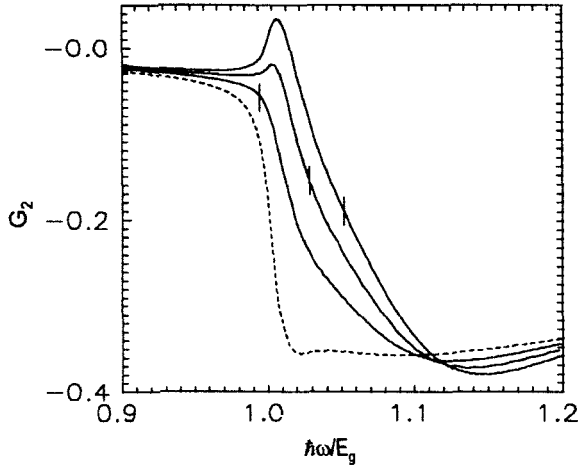
FIG. 11. Calculated dispersion function G_2 for various injected current density levels. The dashed line is for passive material. The transparency point of each curve is marked with a vertical bar. Figure from Sheik-Bahae and Van Stryland (1994).

ism is a simple extension of the TPB theory describing bound-electronic processes in passive semiconductors presented in Section III. The nonlinear refractive index n_2 in the SLA is described by an equation similar to Eq. (52), except that the dispersion function depends not only on $\hbar\omega/E_g$ but also on the lattice temperature (kT/E_g), quasi-Fermi levels set by the injected current density, and broadening due to polarization dephasing $(\hbar/T_2 E_g)$. Figure 11 depicts the calculated dispersion function G_2 for various current injection levels plotted as a function of photon energy normalized to the passive band gap. The dynamic transparency point changes with current density, as indicated by vertical bars in the figure.

The sign and magnitude of the predicted n_2 values are in close agreement with existing experimental results (Haltgren and Ippen, 1991; Haltgren et al., 1992; Grant and Sibbet, 1991). A straightforward comparison can be made between the calculated spectral dispersion function G_2 for a SLA at the transparency point and the value of G_2 for passive material operating just below half the band gap. The comparison indicates that more than an order-of-magnitude enhancement of this function can be obtained with active materials. Note, however, that the nonlinear refraction is determined by the product of the factors G_2 and E_g^{-4}. For a given wavelength, SLA operation requires a band gap that is smaller by about a factor of 2. Therefore, for a fixed wavelength, the two contributions will enhance n_2 for an SLA by more than 2 orders of magnitude compared with a half-band-gap

passive switch (see Section VII.1 on all-optical switching). Recent optical switching experiments using SLA devices have indicated nearly an order of magnitude lower switching power compared with passive NLDC devices (Lee *et al.*, 1994). Further optimization and systematic study of SLA nonlinearities are expected to lower the switching threshold further. Parasitic effects arising from the dynamics discussed earlier introduce complications that need to be considered. A comprehensive theory that self-consistently unifies bound-electronic effects with spectral hole burning and carrier heating is presently not at hand.

V. Free-Carrier Nonlinearities

Besides ultrafast bound-electronic nonlinear effects discussed so far, additional NLA and NLR effects can arise from free carriers generated by multiphoton absorption in the transparency region. These nonlinearities are distinguishable from $\chi^{(3)}$ effects because they are cumulative (with a decay given by the carrier lifetime) and appear as higher-order processes (if the carriers are produced by linear absorption, the resulting nonlinear response is third order, see Chap. 1 in this volume and Chap. 5 in Volume 59). In this chapter we discuss the free-carrier effects mainly to point out their role in complicating the $\chi^{(3)}$ measurement process. In fact, the discrepancies of measured values of 2PA coefficients reported in the literature often can be understood by understanding these effects (Van Stryland and Chase, 1994). For example, in a single-beam experiment, if significant carrier densities are created, the nonlinear absorption equation [Eq. (14) for a single beam] must be modified as follows:

$$\frac{dI}{dz} = -\alpha I - \beta I^2 - (\sigma_e \Delta N_e + \sigma_h \Delta N_h) I \tag{59}$$

where $\sigma_{e,h}$ is the free-carrier absorption (FCA) cross section (units of square centimeters) for electrons and holes, respectively. In many semiconductors described by the Kane model, free-hole absorption dominates (i.e., $\sigma_h \gg \sigma_e$) due to strong inter-valence band absorption. In a two-band approximation, we take $\Delta N_e = \Delta N_h = \Delta N$ and define $\sigma = \sigma_e + \sigma_h$. Assuming 2PA is the only mechanism for generating carriers, and neglecting population decay within the pulse and spatial diffusion, the carrier generation rate is given by

$$\frac{d\Delta N}{dt} = \frac{\beta I^2}{2\hbar\omega} \tag{60}$$

The combination of Eqs. (59) and (60) shows a fifth-order nonlinear response of the loss for carriers generated by 2PA (i.e., N is proportional to

I^2, leading to an I^3 dependence of the loss). The fifth-order response comes from the combination of $\mathscr{I}m\{\chi^{(3)}\}$ followed by a $\chi^{(1)}$ process, either absorption ($\mathscr{I}m\{\chi^{(1)}\}$) or refraction ($\mathscr{R}e\{\chi^{(1)}$. Equation (60) is only valid for pulses short enough that carrier recombination, decay, and diffusion can be ignored. This shows one of the simplifications afforded by using short optical pulses for determining β (or n_2). Another advantage is that short pulses minimize the effects of FCA (and the associated free-carrier refraction), since the energy for a fixed irradiance is reduced [and the less energy, the fewer carriers created, as seen by the temporal integral of Eq. (60)]. The FCA term in Eq. (59) can range from negligible to dominant depending on the semiconductor, wavelength, irradiance, and temporal pulsewidth. For example, for InSb, the FCA terms in Eq. (59) actually dominate the overall loss even for 100-ps, 10.6-μm pulses (Hasselbeck *et al.*, 1997).

Knowledge of the free-carrier absorption coefficient σ allows relatively simple modeling of the overall loss; however, σ often must be determined empirically. Even in situations where the free-carrier losses can be made negligible (e.g., for short pulses), index changes due to the carrier excitation (so-called free-carrier refraction, FCR) can still be significant. This FCR is not simply calculated via KK from the added FCA spectrum. This turns out to be a small contribution to the total NLR. The dominant NLR is instead calculated from the saturation of the interband linear absorption spectrum resulting from the redistribution of electron population. A similar process occurs in a laser where the index change due to gain saturation leads to frequency pulling of the cavity modes (Meystre and Sargent, 1991). The method of carrier excitation is irrelevant to the resulting index change. The removal of electrons from the valence band (creation of electrons in the conduction band) reduces the linear absorption for wavelengths near the band edge (band blocking). This is referred to as the *dynamic Burnstein-Moss shift* (Moss, 1980; Burstein, 1954). Carrier-carrier scattering tends to thermalize the carrier distribution on the time scale of ~ 1 ps, while recombination times are much longer. Therefore, there is a quasi-equilibrium distribution of carriers that reduces the linear absorption by removing potential interband transitions and, via causality, changes the index. The NLR is calculated from the changed absorption spectrum according to Eq. (27). The free-carrier NLR has a negative sign in the transparency region of semiconductors (from the reduced absorption), leading to beam defocusing. In experiments where the carriers are created by linear absorption with near-gap excitation, this NLR can be huge (Miller and Duncan, 1987). Here, where the excitation is by 2PA, we are well below the frequency where the index changes are large, but the effects can still be comparable or even larger than the effects from n_2. The importance of understanding the free-carrier nonlinearities in the transparency region is twofold. On the one hand, it may be useful for applications such as optical limiting (see Section VII.2). On the

other hand, it can complicate the measurement or mask the usefulness of the bound-electronic effect in ultrafast applications such as optical switching.

The effect of these free oscillators on the phase is proportional to the density of created carriers:

$$\frac{d\Phi}{dz} = kn_2 I + k\sigma_r \Delta N \tag{61}$$

which includes the effects of the bound-electronic n_2 as well as the free-carrier refractive coefficient σ_r (units of cubic centimeters). The k in the second term is sometimes dropped to give the refractive cross section in units of square centimeters. This fifth-order nonlinear refraction can be seen in measurements of the induced phase distortion, as shown in Fig. 12. This figure shows the index change divided by the input irradiance I_0 as a function of I_0 in ZnSe at 532 nm, where it exhibits 2PA. The index change is calculated from the measured phase distortion introduced on the beam through propagation in bulk samples. For a purely third-order response, $\Delta n = n_2 I_0$, this figure would show a horizontal line. The slope of the line in Fig. 12 shows a fifth-order response, whereas the intercept gives n_2 (note here that it is negative). The interpretation of this fifth-order response as defocusing from carriers generated by 2PA is consistent with a number of experimental measurements including degenerate four-wave mixing measurements (Canto-Said *et al.*, 1991) and Z-scan and time-resolved two-color Z-scan measurements, as discussed in Section VI (Sheik-Bahae *et al.*, 1992; Wang *et al.*, 1994).
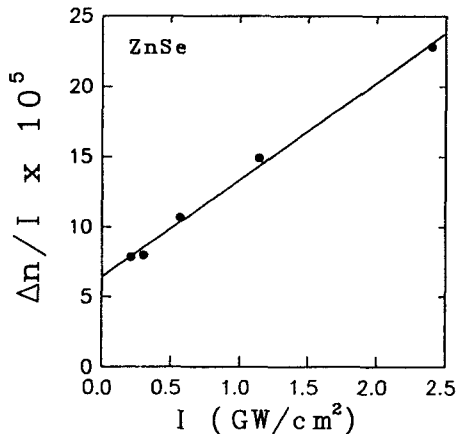

FIG. 12. A plot of the ratio of the change in refractive index to irradiance as a function of irradiance for 532-nm picosecond pulses in ZnSe. Figure from Said *et al.* (1992).

We next look briefly at two different band-filling (BF) models describing this nonlinear refraction. The first model (BF1) is attributed to Aronov *et al.* (1968) and Auston *et al.* (1978), and the second is the dynamic Moss-Burstein model with Boltzmann statistics (BF2) (Moss, 1980; Miller *et al.*, 1981b; Wherrett *et al.*, 1988). In these theories, the change in refraction due to carriers is independent of the means of carrier generation (see Chap. 5 in Volume 59 for more information on carrier nonlinearities). In the BF1 model, the nonlinear refraction due to free carriers is calculated directly from the real part of the complex dielectric function. The creation of a density ΔN of free electrons in the conduction band is accompanied by an elimination of a density N of bound electrons in the valence band. The former is often referred to as the *Drude contribution*, whereas the latter is referred to as a *Lorentz contribution* to the change in the dielectric constant. The overall change in the index of refraction is given by Auston *et al.* (1978)

$$\Delta n(\omega; \Delta N) = \sigma_r \Delta N = -\frac{\Delta N e^2}{2\varepsilon_0 n_0 \omega^2 m_{cv}} \frac{E_g^2}{E_g^2 - (\hbar\omega)^2} \qquad (62)$$

where m_{cv} is the reduced effective mass of the electrons in the conduction band and the holes in the valence band.

In the BF2 model, as was originally introduced by Miller *et al.* (1981), the free carriers block the absorption at frequencies higher than the energy gap by filling the available states in the conduction and valence bands. This model uses a Kramers-Kronig integral on this change in absorption. The total change in the index of refraction using a three-band model, including contributions from electrons, heavy holes, and light holes, is given by (Wherrett *et al.*, 1988) as

$$\Delta n = -\frac{e^2}{2\varepsilon_0 n_0 \omega^2} \left\{ \begin{array}{l} \dfrac{\Delta N_c}{m_c}\left[1 + Z\left(\dfrac{m_{ch}}{m_0}J_{hc} + \dfrac{m_{cl}}{m_0}J_{lc}\right)\right] \\[3mm] + \dfrac{\Delta P_h}{m_h}\left(1 + Z\dfrac{m_{ch}}{m_0}J_{hh}\right) + \dfrac{\Delta P_l}{m_l}\left(1 + Z\dfrac{m_{cl}}{m_0}J_{ll}\right) \end{array} \right\} \qquad (63)$$

where

$$Z = \frac{2}{3\sqrt{\pi}} \frac{E_p}{k_B T} \left(\frac{\hbar\omega}{E_g}\right)^2 \qquad (64)$$

$$J_{ij} = \int_0^x \frac{x^2 \exp(-x^2)}{x^2 + a_{ij}} dx \qquad (65)$$

$$a_{ij} = \frac{E_g - \hbar\omega}{k_B T} \frac{m_{ci}}{m_j} \qquad (66)$$

where m_0 is the free electron mass, k_B is the Boltzmann constant, T is the temperature in degrees Kelvin, and $E_p = 2|p_{cv}(k = 0)|^2/m_0$ is the Kane energy, as discussed in Section III.1, and is approximately 21 eV for most semiconductors (Kane, 1980) ΔN and ΔP represent the photogenerated electron and hole densities, and the subscripts c, h, and l represent the conduction, heavy-hole, and light-hole bands, respectively. Similarly, m_j represents the effective mass of the band j, and m_{ij} denotes the reduced effective mass of the ij band pair. The dummy subscripts i and j represent c, h, or l. ΔP_h and ΔP_l are given by (Wherrett et al., 1988)

$$\frac{\Delta N_c}{\Delta P_h} \cong 1 + \left(\frac{m_l}{m_h}\right)^{3/2} \quad \text{and} \quad \frac{\Delta N_c}{\Delta P_h} \cong 1 + \left(\frac{m_h}{m_l}\right)^{3/2} \tag{67}$$

Expression (63) (with Eq. 65) is an approximation adequate for near-resonance radiation. Off resonance, as in 2PA, we find that J_{ij} should be replaced by F_{ij}, where F is defined as

$$F_{ij} = -2J\left(\frac{m_{ci}}{m_j}\frac{E_g}{k_B T}\right) + J\left(\frac{m_{ci}}{m_j}\frac{E_g - \hbar\omega}{k_B T}\right) + J\left(\frac{m_{ci}}{m_j}\frac{E_g + \hbar\omega}{k_B T}\right) \tag{68}$$

For $\hbar\omega \cong E_g$ and $E_g \gg k_B T$, the first and third terms in Eq. (68) are very small compared with the second term; thus it is reasonable to neglect them (Miller et al., 1981; Wherrett et al., 1988). In 2PA experiments, $E_g \pm \hbar\omega$ is comparable with E_g, and all three terms in Eq. (68) need to be retained.

The electron's contribution to the index change is the first term in Eq. (63) (ΔN_c), and this includes blocking caused by electron transitions from the heavy-hole band and the light-hole band in addition to the change in the electron population in the conduction band. The other two terms give the contributions of the holes. Calculations of the free-carrier refraction using both models give good agreement with data taken on the semiconductors GaAs and CdTe at 1.06 μm, and ZnSe at 532 nm using picosecond pulses (see Fig. 12) (Said et al., 1992). For these materials, both models work well, since the change in the index of refraction from transitions between the light-hole band and the conduction band (electron blocking, light-hole blocking, and free light-hole generation) contributes only about 30% for these semiconductors. Thus it is reasonable to use the approximation of a two-band model where only transitions from heavy-hole band to conduction band are considered. For these materials, the low-temperature condition or $|\hbar\omega - E_g| \gg k_B T$ is satisfied; for example, in the worst case of GaAs, $|\hbar\omega - E_g| = 0.25$ eV, and at room temperature, $k_B T \cong 0.025$ eV. Examining J_{ij} in Eq. (65), $a_{ij} \gg 1$, yielding $J_{ij} \cong \pi^{1/2}/4a$. Substituting this value for J_{ij}

in Eq. (68), F_{ij} is proportional to $x^2/(1 - x^2)$, where $x = \hbar\omega/E_g$. Assuming a two-band model and substituting F_{ij} for J_{ij} in Eq. (65) shows that the change in the index of refraction due to the carrier transition blocking is

$$\Delta n \propto \frac{1}{E_g^2 - (\hbar\omega)^2} \qquad (69)$$

having the same frequency dependence as the enhancement factor in the BF1 model. This is expected because the same physical mechanism is used in both calculations. Following the scaling rules applied for describing n_2 and β in Section III, it is helpful to write a similar relation for free-carrier refraction, namely, σ_r. For example, by replacing the effective mass parameter by $m_0 E_g/E_p$, Eq. (62) can be reexpressed as (Wang et al., 1994)

$$\sigma_r(\omega) = A \frac{E_p}{n_0 E_g^3} H\left(\frac{\hbar\omega}{E_g}\right) \qquad (70)$$

where $A = \hbar^2 e^2/2\varepsilon_0 m_0 = 3.4 \times 10^{-22}\,\text{cm}^3\text{eV}^2$, and $H(x) = [x^2(x^2 - 1)]^{-1}$ is the free-carrier dispersion function. Figure 13 compares this dispersion function with some experimental data properly scaled using $A \approx 2.3 \times 10^{-22}\,\text{cm}^3\text{eV}^2$. The experimental procedure used for these measurements is given in Section VI.7.

Another theory of free-carrier nonlinearities as given by Banyai and Koch (1986) includes the effects of electron-hole Coulomb interaction, plasma screening, and band filling. This theory has been shown to have good
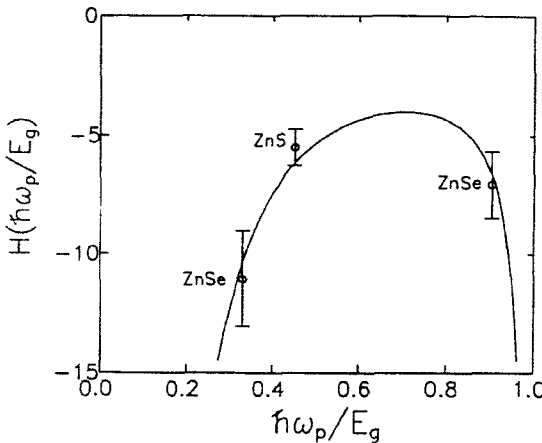

FIG. 13. A plot of $H(x)$ versus x showing free-carrier refraction for three semiconductors as compared with theory (solid line). Figure from Wang et al. (1994).

agreement for near-gap excitation. A quantitative comparison of the predictions of this theory with data taken at frequencies where the excitation is well below the band edge shows poorer agreement (Said *et al.*, 1992).

VI. Experimental Methods

There are a number of experimental difficulties that need to be addressed when attempting to determine the value of ultrafast nonlinearities, $\beta = \alpha_2^{2PA}$ or n_2. For example, an examination of the literature on reported values of β for the single semiconductor GaAs shows well over a 2 order of magnitude variation in the reported value over the past four decades. As mentioned in the preceding section, competing effects of free carriers could easily lead to an overestimation of β as well as an incorrect value of n_2. Using shorter optical pulses minimizes these and other possible cumulative effects; however, even if the cumulative effects are negligible, nonlinear refraction from n_2 can still affect measurements of β, as can β in measurements of n_2. In addition, laser output pulses having unknown temporal or spatial modulation can lead to an underestimation of the irradiance. Therefore, careful characterization of the laser output is necessary. In "thick" samples, beam propagation can lead to irradiance changes from induced phase shifts within the sample. This can be quite difficult to model and properly taken into account. It is normally advisable to work in the "external self-action" (Kaplan, 1969) regime or thin-sample limit so that beam propagation effects within the sample can be ignored. This greatly simplifies interpretation of data because the equation describing nonlinear absorption can be separated from that describing nonlinear refraction, as has been assumed previously in this chapter; i.e., these equations become Eqs. (14) and (15) [or Eqs. (59) and (61) if carrier nonlinearities are included]. Note that since the nonlinear phase shift depends on the irradiance, Eq. (14) (or 59) must first be solved for $I(z)$ in order to solve Eq. (15) (or 61). Even if the sample satisfies the thin-sample approximation, nonlinear refraction has been known to refract light so strongly after the sample that the detector may not collect all the transmitted energy. This again leads to an overestimation of the nonlinear loss. All the preceding effects can contribute to erroneous values of the nonlinear coefficients.

Several experimental techniques are available for measuring the bound-electronic nonlinear response of semiconductors, i.e., β and n_2. We will only briefly discuss a few such methods: transmittance, beam distortion, degenerate four-wave mixing (DFWM), pump/probe techniques, interferometry, and Z-scan along with its derivatives. In general, it is difficult, if not impossible, with any single technique to unambiguously separate the differ-

ent nonlinear responses. These techniques are sensitive to several different nonlinearities at once. Usually several different experiments are necessary, varying parameters such as irradiance and pulse width, to unravel the underlying physics. Clearly, reducing the pulse width, for ultrafast non-linearities should result in a measurement of the same value of β and n_2 for the same irradiance, whereas slower nonlinear responses will change as the pulse width approaches the response time. Unfortunately, from the stand-point of characterization, ultrafast and cumulative nonlinearities often occur together in semiconductors, so a simple separation is not possible

1. TRANSMITTANCE

Single-beam direct transmittance measurements have been a primary method for determining β in semiconductors (Van Stryland et al., 1985a; Bechtel and Smith, 1976). Plots of the inverse transmittance versus irra-diance are nearly straight lines with the intercept determined by α_0 and slope proportional to β. This is seen by solving Eq. (59) neglecting carrier losses, i.e., $\sigma = 0$, giving

$$I(z) = \frac{I(0)e^{-\alpha_0 z}}{1 + \beta I(0) \dfrac{(1 - e^{-\alpha_0 z})}{\alpha_0}} \tag{71}$$

Integrals over the spatial and temporal beam profiles tend to slightly reduce the slope of these plots, as shown in Fig. 14. This figure shows the inverse transmittance of collimated 532-nm pulses incident on a 2.7-mm-thick sample of chemical vapor deposition grown ZnSe as a function of peak on-axis irradiance (Van Stryland et al., 1985a, 1985b). Great care must be taken to ensure that all transmitted light is collected. Two curves are shown for pulse widths of 40 and 120 ps (FWHM). The fact that these two curves lie on top of one another indicates that the cumulative effects of free-carrier absorption are negligible for these pulse widths, and a value of β can be reasonably deduced from these data as shown in Figs. 5 and 6. Longer pulse widths show a clear deviation due to FCA.

2. BEAM DISTORTION

Measurements of n_2 also can be performed in transmission by monitoring the beam distortion that occurs on propagation (Williams et al., 1984). Figure 15 shows the beam distortion in the near field introduced in ZnSe by picosecond 532-nm pulses by the combined effects of 2PA, bound-electronic n_2, and free-carrier refraction (FCR). As determined from a series
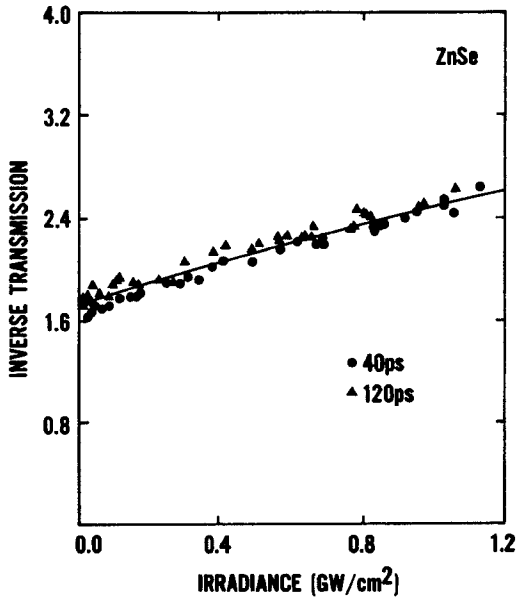
FIG. 14. Inverse transmittance as a function of irradiance of 532-nm picosecond pulses in ZnSe for two different pulse widths. Figure from Van Stryland *et al.* (1985a).
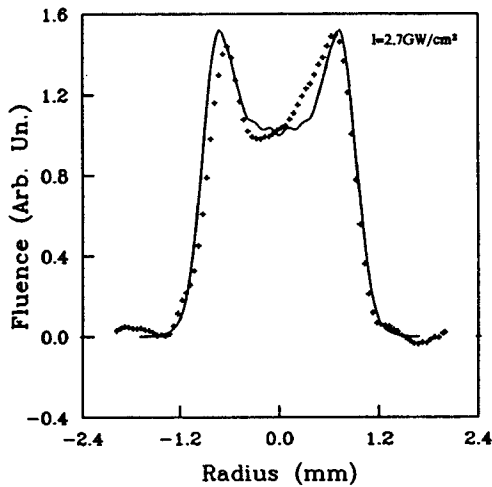
FIG. 15. A one-dimensional spatial profile in the near field of a picosecond 532-nm pulse transmitted through ZnSe. Figure from Van Stryland (1996).

of other experiments (Z-scan and DFWM), both n_2 and the FCR lead to self-defocusing and contribute about equally to the self-lensing shown in Fig. 15 (the solid line is the theory using parameters deduced from other experiments). The sensitivity of this experiment is limited. For example, peak on-axis optical path length changes need to be greater than approximately $\lambda/4$ in order to see changes to a Gaussian beam when propagated to the far field. It is also difficult to separate these different contributions with only beam distortion measurements. Even 2PA alone leads to beam shape changes with propagation. For example, a Gaussian beam is spatially broadened after propagation through a 2PA material because the center portion of the beam is preferentially absorbed, and therefore, the diffraction is reduced. This effect could be mistaken for self-focusing. Sheik-Bahae et al. (1990) and Hermann and Wilson (1993) give details of the modeling of propagation for samples that satisfy the external self-action criteria. Whereas Chapple et al. (1994), Sheik-Bahae et al. (1990), Hermann and McDuff (1993), and Tian et al., (1995), give information on modeling methods for thick samples

3.   EXCITE-PROBE

Pump-probe (or excitation-probe) measurements are useful for studying the temporal dynamics of nonlinear absorption (Shank et al., 1978). In these experiments, an excitation pulse (pump) excites the sample (changes its optical properties), and a probe pulse, spatially coincident with the pump, detects the changes in the optical properties as a function of time delay after the pump. The change in transmittance of a weak probe pulse as a function of time delay after excitation by a short optical pulse allows slow and "fast" nonlinear responses to be separated. The probe is usually derived from the excitation pulse. In the case of equal frequencies (degenerate), the probe is a time-delayed replica and must be separated from the pump either spatially or by using a different polarization. Nondegenerate 2PA can be determined by frequency shifting either the pump or probe, allowing spectral separation of the probe transmittance. Determining whether or not the "fast" response is due to 2PA depends on the laser pulse width used. For picosecond/subpicosecond excitation, one can be reasonably certain that a signal is from multiphoton absorption if it follows the input pulse in time and shows an increasing loss. If in addition the loss varies according to Eq. (70) (a third-order nonlinearity), it is likely due to 2PA.

Nondegenerate nonlinear absorption spectra also have been measured, often using a fixed-frequency laser pump combined with a white-light probe such as the output of a flashlamp (Hopfield et al., 1963). In such a case, the

temporal extent of the white-light source is usually much longer than the laser pulse and is often measuring the spectrum of cumulative nonlinearities, which can be different from the initial 2PA spectrum. The advent of femtosecond white-light continuum generation has allowed nondegenerate spectra to be taken on short time scales, where the ultrafast response dominates (see Section VI.8) (Bolger *et al.*, 1993).

Again, interpretation of the nonlinear response is made difficult by the fact that these pump/probe methods are sensitive to any induced change in loss; however, most induced phase shifts will not give rise to a measurable signal. An experimental geometry that allows index changes to generate large signals is the optical Kerr-Gate. This is a form of pump/probe experiment where induced anisotropy leads to polarization changes (Maker *et al.*, 1964). As discussed next, three-beam interactions can produce a fourth beam through NLA and/or NLR.

4.   FOUR-WAVE MIXING

Four-wave mixing, where three beams are input to a material and a fourth wave (beam) is generated, can be used for determining the magnitude of a material's nonlinear response and its response time. If the response is known to be third-order and ultrafast, $|\chi^{(3)}|$ can be determined along with some of its symmetry properties by varying the relative polarizations of the input beams (as well as by monitoring the polarization of the fourth wave). In addition, the frequencies of the input beams can be changed independently to determine the frequency dependence of the nonlinear response, but this can result in the need for a complex geometry to satisfy phase-matching requirements. Equal frequencies are often used, resulting in a much simpler geometry for phase matching, and this is referred to as *degenerate four-wave mixing* (DFWM). Figure 16 shows one simple geometry for DFWM where two of the input beams (the forward and backward pumps) are oppositely directed. If these beams are nearly plane waves (i.e., well collimated), this geometry ensures phase matching for any third input beam (the signal). Introducing delay arms into each of the beams also allows the temporal dynamics of the nonlinearities to be measured for short optical input pulses. A particularly useful measurement (see Fig. 16) is to monitor the energy of the fourth beam (so-called phase-conjugate beam) as a function of the time delay of the perpendicularly polarized backward pump (signal and forward pump have the same linear polarization) (Fisher, 1983).

Figure 17 shows the results of this experiment performed on a sample of ZnSe using ~ 30-ps, 0.532-μm pulses (Canto-Said *et al.*, 1991). Clearly, two very distinct nonlinearities are evident from this figure. Near zero delay, a
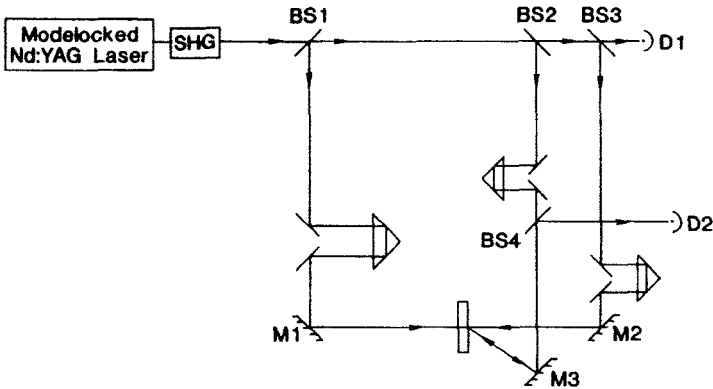
FIG. 16. DFWM geometry to allow temporal dynamics measurements. Detector D_2 monitors the conjugate beam energy. Figure from Canto-Said et al. (1991).

large, rapidly decaying signal is seen that follows the input pulse. At longer delays, we observe a more slowly decaying signal. To better understand the two nonlinear regimes, irradiance-dependent experiments can be performed. The inset in Fig. 17 shows a log-log plot of the DFWM signal versus the total input irradiance (all three input beams are varied simultaneously) at two different delay times. The zero-delay curve gives a power dependence of 3.1 ± 0.2, indicative of a third-order nonlinearity. The curve for a delay of $\sim 200\,\text{ps}$ shows a power law dependence of 5.0 ± 0.2. This is the fifth-order carrier nonlinear refraction discussed in Section V. Here, a modulated carrier density, created by 2PA from the interference of the copolarized forward pump and signal beam, creates a modulation of the refractive index (FCR) that scatters the backward pump into the fourth beam. In principle, free-carrier absorption also will contribute, but other experiments (see Section VI.7) have shown that FCR dominates for these pulse widths. For longer pulses, free-carrier absorption also would contribute to the fifth-order signal. The carrier grating then decays due primarily to diffusion of the carriers between interference fringes as well as some decay by recombination. Studies in CdTe at $1.06\,\mu\text{m}$, where this material exhibits 2PA, reveal the same basic behavior (Canto-Said et al., 1991).

One of the difficulties in the interpretation of DFWM data for third-order nonlinearities is that the signal is proportional to $|\chi^{(3)}|^2 = \mathscr{R}e\{\chi^{(3)}\} + \mathscr{I}m\{\chi^{(3)}\}|^2$, and so 2PA and n_2 both contribute. Separating the effects is difficult without performing additional experiments. Also, as seen in Fig. 17, higher-order nonlinearities also can contribute, making separation of absorptive and refractive effects difficult.
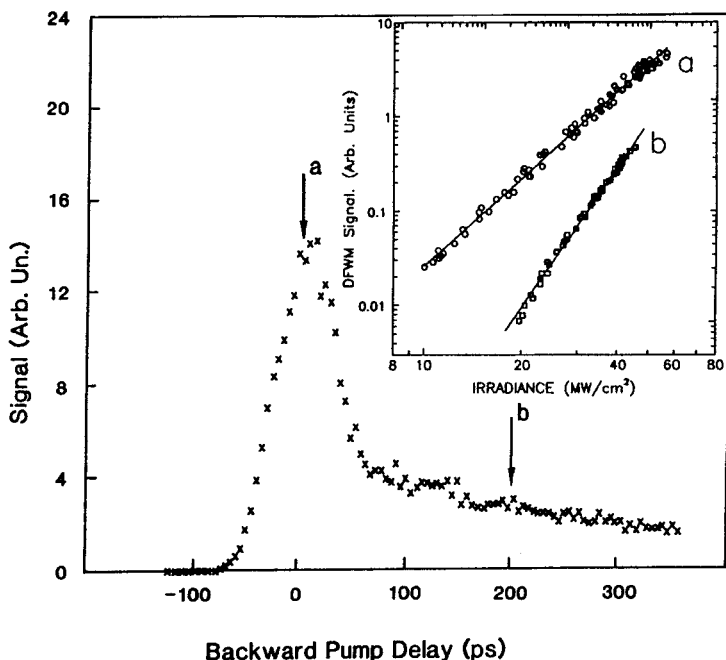
FIG. 17. DFWM signal in ZnSe for temporally coincident, copolarized, forward pump, and probe as a function of the time delay of the perpendicularly polarized backward pump. The inset shows a log-log plot of the output signal as a function of the input (all three inputs varied) for (a) zero temporal delay and (b) ~200-ps delay. Figure from Canto-Said et al. (1991).

5. INTERFEROMETRY

A number of interferometric methods have been used to measure non-linearly induced phase distortion (Adair et al., 1989; Weber et al., 1978; Moran et al., 1975; Xuan et al., 1984). Often a sample is placed in one path (e.g., arm) of an interferometer, and the interference fringes are monitored as a function of irradiance. For example, if the interferometer is first set to give a series of straight-line interference fringes for low input (linear regime), the fringes become curves at high inputs near the central, high-irradiance portion of the beam. The addition of a streak camera can add time resolution to the analysis (Moran et al., 1975). Alternatively, a third beam pathway can be added so that fringes from two weak beams are monitored and the sample is in the path of one weak beam and the strong third beam. Then the fringe shift occurs when the strong beam is blocked and un-blocked, giving the optical path-length change from which the phase shift

can be determined (Xhan *et al.*, 1984). Interferometric methods require good stability and precise alignment; however, such techniques using various modulation schemes have resulted in sensitivities of better than $\lambda/10^4$ in the induced optical path-length changes.

6. Z-SCAN

Z-scan was developed for measuring nonlinear refraction (NLR) and determining its sign (Sheik-Bahae *et al.*, 1989). It was soon realized that it also was useful for measuring nonlinear absorption (NLA) and separating the effects of NLR from NLA (Sheik-Bahae *et al.*, 1990). We start by explaining its use for determining NLR. Using a single focused beam, as depicted in Fig. 18, we measure the transmittance of a sample through an aperture (Z-scan) or around an obscuration disk (EZ-scan) (Xia *et al.*, 1994; Van Stryland *et al.*, 1994), where either are positioned in the far field. The transmittance is determined as a function of the sample position Z measured with respect to the focal plane. Using a Gaussian spatial profile beam simplifies the analysis. The following example qualitatively describes how such data (Z-scan or EZ-scan) are related to the NLR of the sample.

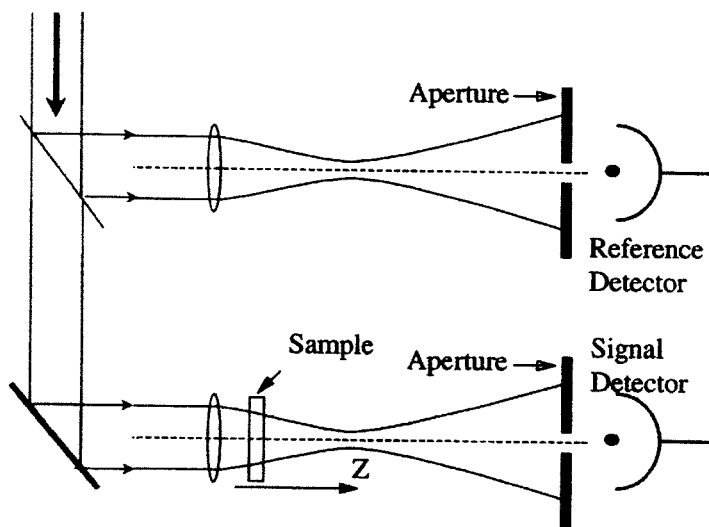Assume, for example, a material with a positive nonlinear refractive index.

FIG. 18.   Z-scan geometry with reference detector to minimize background and maximize the signal-to-noise ratio. Figure adapted from Sheik-Bahae *et al.* (1989).
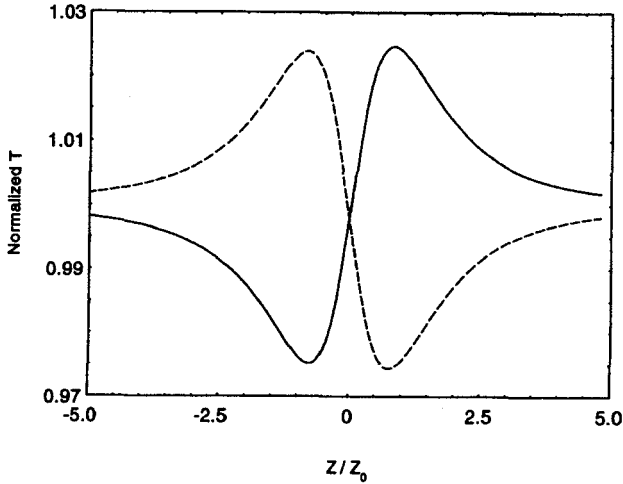
FIG. 19. Predicted Z-scan signal for positive (solid line) and negative (dashed line) nonlinear phase shifts.

Starting the Z-scan (i.e., aperture) from a distance far away from the focus (negative Z), the beam irradiance is low, and negligible NLR occurs; hence the transmittance remains relatively constant. The transmittance here is normalized to unity, as shown in Fig. 19. As the sample is brought closer to focus, the beam irradiance increases, leading to self-focusing in the sample. This positive NLR moves the focal point closer to the lens, leading to a larger divergence in the far field. Thus the aperture transmittance is reduced. Moving the sample to behind the focus, the self-focusing helps to collimate the beam, increasing the transmittance of the aperture. Scanning the sample further toward the detector returns the normalized transmittance to unity. Thus the valley followed by peak signal is indicative of positive NLR, whereas a peak followed by a valley shows self-defocusing. Figure 19 shows the expected result for both negative and positive self-lensing. The EZ-scan reverses the peak and valley because, in the far field, the largest fractional changes in irradiance occur in the wings of a Gaussian beam. The EZ-scan can be more than an order-of-magnitude more sensitive than the Z-scan.

We can define an easily measurable quantity ΔT_{pv} as the difference between the normalized peak and valley transmittance: $T_p - T_v$. The variation of ΔT_{pv} is found to be linearly dependent on the temporally averaged induced phase distortion, defined here as $\Delta \Phi_0$ [for a bound-electronic n_2, $\Delta \Phi_0$ involves a temporal integral of Eq. (61) without carrier refraction, i.e., $\sigma_r = 0$] (Sheik-Bahae et al., 1990b). For example, in a Z-scan using a small

aperture with a transmittance of $S < 10\%$,

$$\Delta T_{pv} \cong 0.41|\Delta\Phi_0| \qquad \text{for } \Delta T_{pv} < 1 \tag{72}$$

assuming CW illumination. With experimental apparatus and data-acquisition systems capable of resolving transmission changes $\Delta T_{pv} \cong 1\%$, Z-scan is sensitive to less than $\lambda/250$ wavefront distortion (i.e., $\Delta\Phi_0 = 2\pi/250$). The Z-scan has a demonstrated sensitivity to a nonlinearly induced optical path-length change of nearly $\lambda/10^3$, whereas the EZ-scan has shown a sensitivity of $\lambda/10^4$, including temporal averaging over the pulse width. Here the temporal averaging for an instantaneous nonlinearity and Gaussian temporal shape gives $\Delta\Phi_0 = \Delta\Phi_{\text{peak}}/\sqrt{2}$, whereas for a long-lived nonlinearity (much longer than the pulse width), $\Delta\Phi_0 = \Delta\Phi/2$ independent of the pulse shape.

In the preceding picture we assumed a purely refractive nonlinearity with no absorptive nonlinearities such as 2PA that will suppress the peak and enhance the valley. If NLA and NLR are present simultaneously, a numerical fit to the data can in principle extract both the nonlinear refractive and absorptive coefficients. However, a second Z-scan with the aperture removed and care taken to collect all the transmitted light can determine the NLA independently. For 2PA alone and a Gaussian input beam, the loss nearly follows the symmetric Lorentzian shape as a function of the sample position Z. The magnitude of the loss determines the NLA, e.g., β from Eq. (71). This so-called open aperture Z-scan is only sensitive to NLA. A further division of the apertured Z-scan data (referred to as *closed-aperture* Z-scan) by the open-aperture Z-scan data gives a curve that for small nonlinearities is purely refractive in nature (Sheik-Bahae *et al.*, 1990b). In this way we have separate measurements of the absorptive and refractive nonlinearities without the need for computer fits of the Z-scans. Figure 20 shows such a set of Z-scans for ZnSe. Here the lines are numerical fits to the curves. Separation of these effects without numerical fitting for the EZ-scan is more complicated.

7. EXCITE-PROBE Z-SCAN

Excite-probe techniques in nonlinear optics have been employed to deduce information that is not accessible with a single-beam geometry (Shank *et al.*, 1978). By using two collinear beams in a Z-scan geometry, we can measure nondegenerate nonlinearities, we can temporally resolve these nonlinearities, and we can separate the absorptive and refractive contributions. There have been several investigations that have used Z-scan in an
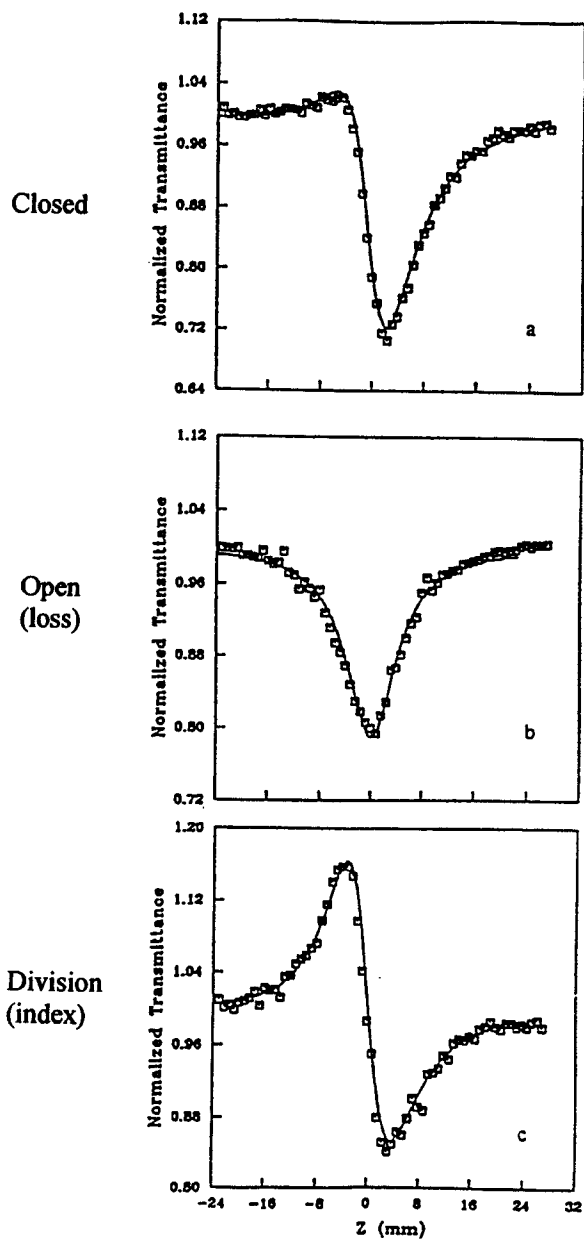
Closed

Open
(loss)

Division
(index)

FIG. 20. Z-scans for ZnSe using picosecond 532-nm pulses: (a) open aperture; (b) closed aperture; (c) closed aperture data divided by open aperture data. Figure adapted from Sheik-Bahae *et al.* (1991).

excite-probe scheme. Z-scan can be modified to give nondegenerate non-
linearities by focusing two collinear beams of different frequencies into the
material and monitoring only one of the frequencies (different polarizations
can be used for degenerate frequencies) (Ma et al., 1991; Sheik-Bahae et al.,
1992). The general geometry is shown in Fig. 21. After propagation through
the sample, the probe beam is then separated and analyzed through the
far-field aperture. Due to collinear propagation of the excitation and probe
beams, we are able to separate them only if they differ in wavelength or
polarization. The former scheme, known as a *two-color Z-scan*, has been
used to measure the nondegenerate n_2 and β in semiconductors. Figure 22
shows results of such experiments performed on ZnSe and ZnS samples with
excitation at $1.06\,\mu m$ and probing at 532 nm, i.e., $\beta(2\omega; \omega)$ and $n_2(2\omega; \omega)$
(Sheik-Bahae et al., 1994). The data are scaled as before (see Eqs. 51 and 55)
and plotted to show comparison with the TPB model for F_2^{2PA} and G_2.

The most significant application of excite-probe techniques in the past
concerned the ultrafast dynamics of nonlinear optical phenomena. The
two-color Z-scan can separately monitor the temporal dynamics of NLR
and NLA by introducing a temporal delay in the path of one of the input
beams. These time-resolved studies can be performed in two fashions. In one
scheme, Z-scans are performed at various fixed delays between excitation
and probe pulses. In the second scheme, the sample position is fixed (e.g., at
the peak or the valley position), while the transmittance of the probe is
measured as the delay between the two pulses is varied. Figure 23 shows the
result of using this second method on ZnSe to separately determine the
dynamics of the NLA and NLR (i.e., the time-dependent signal at the valley
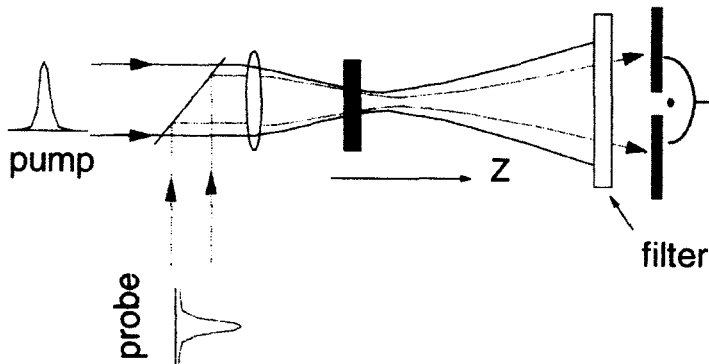is subtracted from that at the peak) [Wang et al., 1994]. The analysis of

FIG. 21. Optical geometry for a two-color Z-scan. The filter blocks the pump beam.
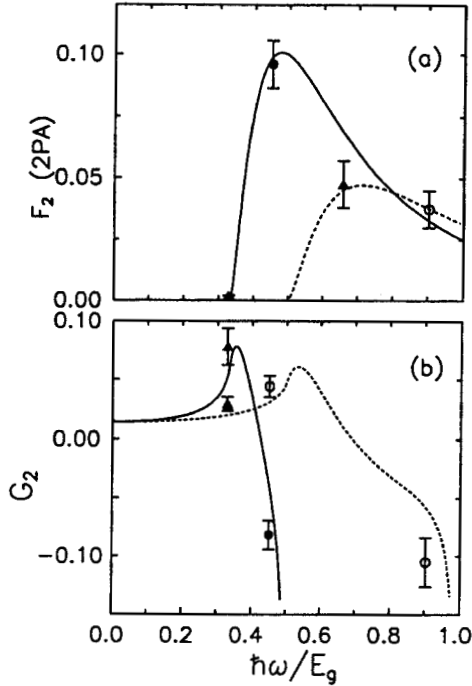Adapted from Sheik-Bahae et al. (1992).

FIG. 22.   (a) The measured degenerate $\beta(2\omega; 2\omega)$ (open symbols) and nondegenerate $\beta(2\omega; \omega)$ (solid symbols) for ZnSe (circles) and ZnS (triangles) using $\omega = 2\pi c/\lambda$ with $\lambda = 1.06\,\mu m$. The data are scaled according to Eq. (51) to compare with the TPB theory; $F_2(2x; x)$ (solid line) and $F_2(x; x)$ dashed line. (b) The corresponding measured n_2 values scaled according to Eq. (55) to compare with the TPB theory; $G_2(2x; x)$ (solid line) and $G_2(x_i x)$ (dashed line). Figure from Sheik-Bahae *et al.* (1992).

two-color Z-scans is naturally more involved than that of a single-beam Z-scan. The measured signal, in addition to being dependent on the parameters discussed for the single-beam geometry, also will depend on parameters such as the excite-probe beam waist ratio, pulse-width ratio, and the possible focal separation due to chromatic aberration of the lens (Wang *et al.*, 1994; Ma *et al.*, 1991; Sheik-Bahae *et al.*, 1992). Table III gives the results of data for ZnSe taken using transmittance, beam distortion, Z-scan, two-color Z-scan, and time-resolved excite-probe techniques.

Another excite-probe technique based on Z-scan geometry is the method of Kerr-lens autocorrelation (Sheik-Bahae, 1997; Sheik-Bahae and Ebrahimzadeh, 1997) suitable for measurements employing femtosecond laser pulses.
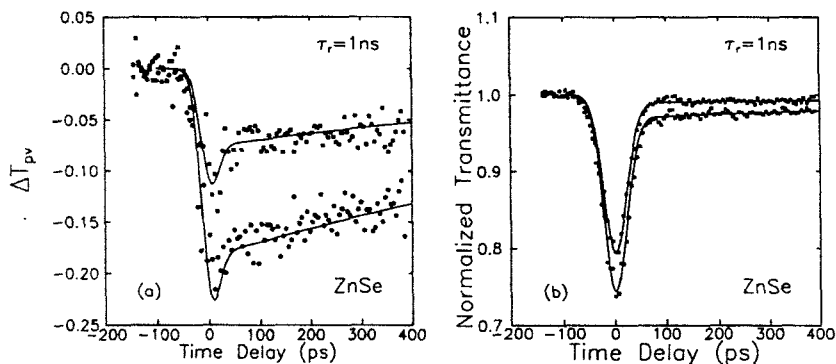
FIG. 23. Time-resolved Z-scan data on ZnSe using 532-nm, picosecond excitation pulses and probing at 1.06 μm: (a) nonlinear refraction versus temporal delay; (b) nonlinear absorption versus temporal delay. Figure from Wang *et al.* (1994).

TABLE III

DATA TAKEN ON CVD-GROWN ZnSe AND ZnS USING SEVERAL OF THE TECHNIQUES DISCUSSED IN THIS SECTION

	ZnSe	ZnS
$\beta(1.06; 1.06)$	0	0
$\beta(0.532; 0.532)$	5.8 ± 1 cm/GW	3.4 ± 0.7 cm/GW
$\beta(0.532; 1.06)$	15 ± 3 cm/GW	0
$\beta(1.06; 0.532)$	4.6 ± 1 cm/GW	0
$\beta^{xy}(1.06; 0.532)$	8.6 ± 2 cm/GW	0
$n_2(1.06; 1.06)$	$(2.9 \pm 0.3) \times 10^{-14}$ cm^2/W	$(6.3 \pm 1.4) \times 10^{-15}$ cm^2/W
$n_2(0.532; 0.532)$	$(-6.8 \pm 1.4) \times 10^{-14}$ cm/W	Not measured
$n_2(0.532; 1.06)$	$(-5.1 \pm 0.5) \times 10^{-15}$ cm^2/W	$(1.7 \pm 0.4) \times 10^{-14}$ cm^2/W
$n_2^{xy}(0.532; 1.06)$	$(-2.6 \pm 0.3) \times 10^{-14}$ cm^2/W	Not measured
$n_2(1.06; 0.532)$	$(-9 \pm 5) \times 10^{-15}$ cm^2/W	$<1.5 \times 10^{-14}$ cm^2/W
$\sigma_a(1.06)$	$(4.4 \pm 1.3) \times 10^{-18}$ cm^2	$(7 \pm 2) \times 10^{-18}$ cm^2
$\sigma_r(1.06)$	$(-6.1 \pm 1.5) \times 10^{-22}$ cm^3	$(5.2 \pm 1.1) \times 10^{-22}$ cm^3
τ	$\sim 10^{-9}$ s	$\tau_a \approx 0.6$ ns; $\tau_r \approx 0.8$ ns

Note: The *xy* superscript indicates that the two beams in the two-color Z-scan were perpendicularly polarized. The τ_a and τ_r for ZnS indicate that the decays seen in the time-resolved two-color Z-scan for absorption and refraction were different.

8.   FEMTOSECOND CONTINUUM PROBE

The development of high-irradiance, femtosecond pulsed laser systems has allowed a pump/probe experiment that automatically yields the non-

degenerate nonlinear absorption spectrum. In such an experiment, the femtosecond pulse is split in two, and one beam is used as the excitation, while the other beam is focused into a suitable material to produce a white-light continuum (Bolger et al., 1993). This white-light continuum is then used as the probe at all frequencies ω' in Eq. (29). Given a sufficiently broad spectrum, the KK integral can be applied to yield the nondegenerate n_2. This method has not been applied to date over a broad spectral range. However, in principle, both nondegenerate β and n_2 can be obtained in a single shot measurement.

9. INTERPRETATION

The interpretation of NLA and NLR measurements is fraught with many pitfalls and great care must be taken. In extensive studies of a wide variety of materials, it is found that there is seldom a single nonlinear proces occurring. Often several processes occur simultaneously, sometimes in unison and sometimes competing. It is necessary to experimentally distinguish and separate these processes in order to understand and model the interaction. There are a variety of methods and techniques for determining the nonlinear optical response, each with its own weaknesses and advantages. In general, it is advisable to use as many complementary techniques as possible over as broad a spectral range as possible to unambiguously determine the active nonlinearities. Numerous techniques are known for measurements of NLR and NLA in condensed matter, including the methods discussed earlier. Nonlinear interferometry (LaGasse et al., 1990; Weber et al., 1978; Moran et al., 1975; Xuan et al., 1984), degenerate four-wave mixing (DFWM) (Canto-Said et al., 1991; Fisher, 1983), nearly degenerate three-wave mixing (Adair et al., 1989), ellipse rotation (Owyoung, 1973), beam distortion (Williams, 1984), beam deflection (Bertolotti, 1988), and third-harmonic generation (Kajzar and Messier, 1987) are among the techniques frequently reported for direct or indirect determination of NLR. Z-scan is capable of separately measuring NLA and NLR (Sheik-Bahae et al., 1989, 1990b). Other techniques for measuring NLA include transmittance (Bechtel and Smith, 1976), calorimetry (Bass et al., 1979), photoacoustic (Bae et al., 1982; Van Stryland et al., 1980), and excite-probe (Shank et al., 1978) methods.

VII. Applications

Ultrafast nonlinearities in optical solids have been used for applications ranging from ultrashort laser pulse generation (Kerr-lens mode locking) to

soliton propagation in fibers over distances of the earth's circumference. Here we briefly discuss two areas of research using optical nonlinearities in the transparency region of semiconductors: (1) all-optical switching, a potential device application in telecommunications switching and routing systems, and (2) optical limiting, primarily applicable to protecting optical sensors from high-irradiance inputs.

1. ULTRAFAST ALL-OPTICAL SWITCHING USING BOUND-ELECTRONIC NONLINEARITIES

An important application of the n_2-β theory that was presented in Section III is that it allows direct determination of the ideal operating point of a passive optical switch. Optical switch designers have established a figure of merit (FOM) for candidate materials, defined by the ratio $\pi n_2/\beta\lambda = 1/T$ (where T is the FOM defined in Mizrahi et al., 1984). The goal of maximizing the FOM clearly shows the need for a large nonlinear phase shift $(\pi n_2/\lambda)$ while keeping the 2PA loss (β) small. By substituting Eqs. (48) and (52) in the FOM ratio, the theory can be used to obtain a universal FOM curve. This FOM is then given by $x G_2(x)/F_2(x) = 1/T$, where $x = \hbar\omega/E_g$. Figure 23 depicts the calculated FOM and a comparison with experimental data obtained for several semiconductors (Sheik-Bahae et al., 1991). The remarkable agreement between theory and experiment indicates that this quantity is indeed a fundamental property of semiconductors, depending only on the normalized optical frequency $(\hbar\omega/E_g)$.

The two horizontal lines in Fig. 24 represent the minimum acceptable FOM for nonlinear directional couplers (NLDC) and Fabry-Perot (FP) interferometers. Although it demands a larger FOM, the NLDC scheme is the preferred practical geometry. From Fig. 24 we see that the FOM requirement is satisfied either just below the 2PA edge or very near resonance $(\hbar\omega \approx E_g)$. Since $n_2 \propto E_g^{-4}$, a low switching threshold at a given wavelength demands a material with the smallest possible band-gap energy. The theory then suggests that the ideal operating region is just below the band gap. However, operation near the band gap forces the designer to contend with increasing loss due to band-tail linear absorption, which makes this scheme unworkable at present (at least in passive material). If operation near the half band gap is contemplated instead, one must pay the penalty of reduced nonlinear refraction (~ 16 times at a given wavelength). To compensate, the operating irradiance must be increased. At high irradiance, however, nonlinear absorption associated with 2PA becomes an issue, making this option problematic as well. Therefore, passive all-optical switching presents fundamental constraints that cannot readily be solved by
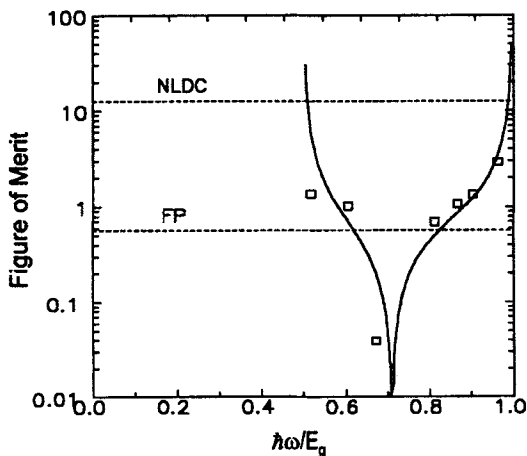
FIG. 24.   Ratio of $n_2/k\beta$ (switching parameter or figure of merit) as a function of $\hbar\omega/E_g$. The solid line is predicted from the two-parabolic-band model. NLDC stands for nonlinear directional coupler, and FP stands for Fabry-Perot etalon. Figure from Sheik-Bahae et al. (1991).

materials engineering. One method being pursued is operating just below the 2PA edge so that 3PA is the dominant loss mechanism. This has led to some promising results (Stegeman et al., 1996). Another method, as discussed previously, is using semiconductor laser amplifiers (SLA), where parasitic linear loss can be mitigated, making near-gap operation a practical possibility.

2.   OPTICAL LIMITING

Passive optical limiting uses a material's nonlinear response to block the transmittance of high-irradiance light while allowing low-irradiance light to be transmitted (an operation similar to that of photochromic sunglasses). The primary application of optical limiting is to protect sensitive optical components from being damaged by the high-intensity input light. The ideal optical limiter has a high linear transmission for low inputs (e.g., energy), a variable limiting input energy, and a large dynamic range defined as the ratio of the linear transmittance to the minimum transmittance obtained for high input (prior to irreversible damage) (Crane et al., 1995; Sutherland et al., 1997). Since a primary application of optical limiting is to protect sensors, and fluence (energy per unit area) almost always determines

damage to detectors; this is the quantity of interest for the output of a limiter. Getting this type of response is possible using a wide variety of materials; however, it is very difficult to get the limiting threshold as low as is often required and at the same time have a large dynamic range. Because high transmission for low inputs is desired, we must have low linear absorption. These criteria lead to the use of materials displaying strong 2PA and nonlinear refraction. Devices based on these nonlinearities can be made to have low limiting thresholds, large dynamic ranges, and broad spectral responses; however, since 2PA and n_2 are irradiance-independent, they work best for short input pulses (Hagan *et al.*, 1988). For example, a monolithic ZnSe device limits the output fluence at input energies as low as 10 nJ (300 W peak power) and has a dynamic range greater than 10^4 for 532-nm, 30-ps (FWHM) pulses, as shown in Fig. 25 (Van Stryland *et al.*, 1988). While the nonlinear response of this device is initiated by 2PA, free-carrier defocusing greatly assists the limiting of the transmitted fluence and is responsible for increasing the dynamic range over which semiconductor limiting devices operate without damage. Since the light is focused in the bulk of the material (see inset of Fig. 25), the semiconductor could itself be damaged. However, at high inputs, the combination of 2PA loss and carrier defocusing that counteracts linear focusing protects the focal position from damage. For longer-pulse operation, however, the dynamic range is significantly reduced. This occurs because the energy input for the same irradiance

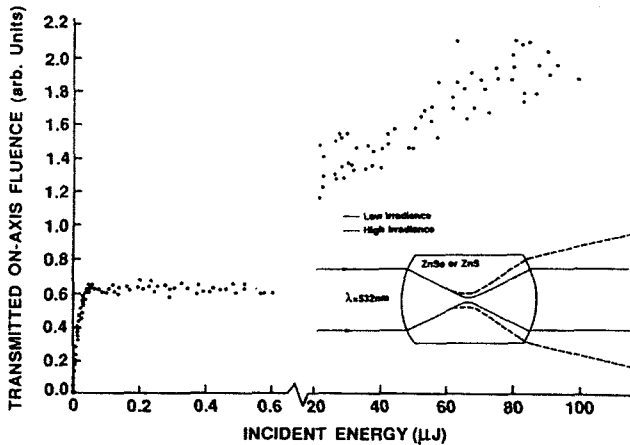

FIG. 25.   Optical limiting data for the monolithic ZnSe lens (~ 3 cm long) shown in the inset for picosecond, 532-nm pulses as a function of the input energy as measured though an aperture approximately 2.5 m after the sample. Adapted from Van Stryland *et al.* (1988).

is increased for longer pulses. While more carriers are generated and free-carrier absorption also becomes significant, they may decay during the pulse, and the energy from nonlinear absorption heats the bulk of the sample. This heat raises the refractive index in most semiconductors. The increase in refractive index causes self-focusing that counteracts the free-carrier defocusing and the sample damages. As seen from the 2PA scaling relations, the 2PA can be greatly enhanced for infrared wavelengths where smaller band-gap energies can be used ($\beta \propto E_g^{-3}$). For example, InSb at $10\,\mu m$ has $\beta \cong 10^4$ cm/GW, and the free-carrier absorption and refraction are very large, dominating the nonlinear response. This material has great potential for sensor protection in the IR (Hasselbeck et al., 1993).

VIII. Conclusion

Since the advent of high-peak-power short-pulse lasers, numerous measurements of the ultrafast optical Kerr effect (n_2) in many semiconductors and large-gap dielectrics have been reported. The experimental techniques used for these measurements range from nonlinear wave mixing to nonlinear interferometry. Almost all the early measurements were obtained in the long-wavelength limit, where n_2 is positive and nondispersive. More recent measurements have shown the dispersive nature of the nonlinear refraction (Sheik-Bahae et al., 1991).

A simple two-band model calculation gives a universal band-gap scaling and dispersion of the electronic Kerr effect in solids. A direct relationship links the nonlinear refractive index n_2 to its nonlinear absorptive counterparts: two-photon absorption, Raman, and AC Stark effects. This theory builds from a large base of existing calculations where nonlinear absorption is calculated by means of transition rates. An appropriate Kramers-Kronig transformation approach is used to obtain the nonlinear refraction in terms of this nonlinear absorption. The power of this approach is that it circumvents the need for a direct calculation of the complex nonlinear susceptibility. It is necessary, however, to know the nondegenerate nonlinear absorption coefficient in order to apply the Kramers-Kronig transformation, i.e., the nonlinear absorption in the material at all frequencies ω_1 in the presence of a strong optical field at ω_2. The n_2 calculation is also performed for the general nondegenerate case where an expression for $n_2(\omega_1; \omega_2)$ is derived. This is the coefficient of nonlinear refractive index at ω_1 due to the presence of a strong optical excitation at ω_2. The well-known and well-studied degenerate n_2 is treated as a special case. Comparing the experimentally measured values of the degenerate n_2 with the theoretical dispersion,

there is good agreement obtained over a wide range of frequencies and materials with a single fitting parameter K'. We note, however, that the theoretical value for this parameter is a factor of 2 to 3 smaller than the empirical value of K'. This underestimation may be expected because the heavy-hole valence band, as well as the electron-hole Coulomb (exciton) interaction, is ignored in this simple theory (Sheik-Bahae *et al.*, 1994). It is also remarkable that the two-band theory gives reasonable agreement with data for large-gap dielectric materials. The theory for passive semiconductors also can be extended to active semiconductor devices, semiconductor laser amplifiers (SLA). The measured sign and magnitude of n_2, as well as the variation of n_2 with injection current density in SLA systems, is in good agreement with calculations.

While the ultrafast nonlinearities of semiconductors can now be predicted with reasonable accuracy given the band-gap energy, linear index, and photon energy, other nonlinearities are often important for device applications. In particular, free-carrier and thermal nonlinearities can significantly alter the nonlinear operation. In practice, the shorter the input pulse, the less these nonlinearities interfere with the simple modeling of the ultrafast response. This occurs because the shorter the pulse, the less energy for a given irradiance and, therefore, the fewer carriers are produced and the less heat is generated.

We end our discussion with a reminder of the difficulties in characterizing the nonlinear optical properties of materials and in particular semiconductors. For example, for photon energies near the band edge, there can be significant linear absorption, and this linear absorption leads to the creation of free carriers that can subsequently absorb and refract light. The refractive component is the more interesting for applications and this resonant nonlinear refraction gives one of the largest nonlinearities ever reported (Miller and Duncan, 1987). However, it and the associated NLA can interfere with the determination of either two-photon absorption or n_2 (we restricted our definition of n_2 to the ultrafast optical Kerr effect from the bound electrons). Without knowledge of the temporal dynamics, both nonlinearities result in a third-order response. In a similar fashion, nonlinear absorption and nonlinear refraction from 2PA-generated carriers result in a fifth-order nonlinearity that is difficult to distinguish from three-photon absorption and "n_3," the fifth-order bound-electronic nonlinear refraction. In all of this, of course, are the problems associated with the interactions between nonlinear loss and nonlinear refraction with multiple sources of nonlinearities; e.g., nonlinear absorption leads to beam-profile changes that alter the propagation, and nonlinear refraction through propagation alters the beam profile. In short, great care must be taken to determine the underlying physics associated with nonlinearities in semiconductors (and other materials).

LIST OF ABBREVIATIONS AND ACRONYMS

2PA	two photon absorption	*hh*	heavy-hole
AOS	all-optical switching	KK	Kramers-Kronig
BF	band-filling	*lh-c*	light-hole-to-conduction band
CW	continuous wave	NLA	nonlinear absorption
DFWM	degenerate four-wave mixing	NLDC	nonlinear directional couplers
FCA	free-carrier absorption	NLR	nonlinear refraction
FCR	free-carrier refraction	QSE	quadratic optical Stark effect
FP	Fabry-Perot	SLA	semiconductor laser amplifier
FOM	figure of merit	TPB	two-parabolic band

REFERENCES

Adair, R., Chase, L. L., and Payne, S. A. (1987). "Nonlinear Refractive-Index Measurements of Glasses Using Three Wave Frequency Mixing," *J. Opt. Soc. Am. B* **4**, 875–881.

Adair, R., Chase, L. L., and Payne, S. A. (1989). "Nonlinear Refractive Index of Optical Crystals," *Phys. Rev. B* **39**, 3337–3350.

Agrawal, G. P. (1989). *Nonlinear Fiber Optics*, Academic Press.

Akhmanov, S. A., Khokhlov, R. V., and Sukhorokov, A. P. (1968). "Self-Focusing and Diffraction of Light in a Nonlinear Medium," *Soc. Phys. Usp.* **10**, 609.

Aronov, A. G., Pikus, D. E., and Shekhter, D. S. (1968). 'Quantum Theory of Free-Electron Dielectric Constant in Semiconductors," *Sov. Phys.-Solid State* **10**, 645.

Auston, D. H., McAffee, S., Shank, C. V., Ippen, E. P., and Teschke, O. (1978). "Picosecond Spectroscopy of Semiconductors," *Solid State Electron.* **21**, 147–150.

Aversa, C., Sipe, J. E., Sheik-Bahae, M., and Van Stryland, E. W. (1994). "Third-Order Optical Susceptibilities in Semiconductors: The Two-Band Model," *Phys. Rev. B* **50**, 18073–18082.

Bae, Y., Song, J. J., and Kim, Y. B. (1982). "Photoacoustic Study of Two-Photon Absorption in Hexagonal ZnS," *J. Appl. Phys.* **53**, 615.

Balterameyunas, R., Vaitkus, Y., Vishchakas, Y., Gavryushin, V., Kubertavichyus, V., and Rachyukaitis, G. (1982). "Spectral and Polarization Investigations of Two-Photon Absorption in Semiconductors of Group A^2B^6 Symmetry," *Izvestiya Akademii Nauk SSSR, Seriya Fizicheskaya*, **46**, 1442–1451.

Banyai, L. and Koch, S. W. (1986). "A Simple Theory for the Effects of Plasma Screening on the Optical Spectra of Highly Excited Semiconductors," *Z. Phys. B* **63**, 283–291.

Bass, M., Van Stryland, E., and Stewart, A. (1979). "Laser Calorimetric Measurement of Two-Photon Absorption," *Appl. Phys. Lett.* **34**, 142.

Bassani, F. and Scandolo, S. (1991). "Dispersion Relations and Sum Rules in Nonlinear Optics," *Phys. Rev. B* **44**, 8446–8453.

Bechtel, J. H. and Smith, W. L. (1976). "Two-Photon Absorption in Semiconductors with Picosecond Pulses," *Phys. Rev. B* **13**, 3515.

Bertolotti, M., Ferrari, A., Sibilia, C., Suber, G., Apostol, D., and Jani, P. (1988). "Photothermal Deflection Technique for Measuring Thermal Nonlinearities in Glasses," *Appl. Phys.* **27**, 1811.

Bolger, J., Kar, A. K., Wherrett, B. S., DeSalvo, R., Hutchings, D. C., and Hagan, D. J., (1993) "Nondegenerate Two-Photon Absorption Spectra of ZnSe, ZnS, and ZnO," *Optics Commun.* **97**, 203.

Boyd, R. W. (1992). *Nonlinear Optics.* Academic Press, San Diego.

Brandi, H. S. and de Araujo, C. B. (1983). "Multiphoton Absorption Coefficients in Solids: A Universal Curve," *J. Phys. C* **16**, 5929–5936.

Braunstein, R. and Ockman, N. (1964). "Optical Double-Photon Absorption in CdS," *Phys. Rev.* **134**, A499–A507.

Burstein, E. (1954). *Phys. Rev.* **93**, 632.

Canto-Said, E. J., Hagan, D. J., Young, J., and Van Stryland, E. W. (1991). "Degenerate Four-Wave Mixing Measurements of High Order Nonlinearities in Semiconductors," *J. Quantum Electron.* **QE-27**, 2274–2280.

Caspers, P. J. (1964). "Dispersion Relations for Nonlinear Response," *Phys. Rev. A* **133**, 1249.

Chapple, P. B., Staromlynska, J., and McDuff, R. G. (1994). "Z-Scan Studies in the Thin- and the Thick-Sample Limits," *J. Opt. Soc. Am. B* **11**, 975–982.

Cotter, D., Burt, M. G., and Manning, R. J. (1992). "Below Band-Gap Third-Order Optical Nonlinearity of Nanometer-Size Semiconductor Crystallites," *Phys. Rev. Lett.* **68**, 1200.

Crane, R., Lewis, K., Van Stryland, E., and Khosnevisan, M. eds. (1995). *Materials for Optical Limiting.* Materials Research Society, Pittsburgh.

DeSalvo, R., Sheik-Bahae, M., Said, A. A., Hagan, D. J., and Van Stryland, E. W. (1993). "Z-Scan Measurements of the Anisotropy of Nonlinear Refraction and Absorption in Crystals," *Opt. Lett.* **18**, 194–196.

Dvorak, M. D., Schroeder, W. A., Anderson, D. R., Smirl, A. L., and Wherrett, B. S. (1994). "Measurement of the Anisotropy of Two-Photon Absorption Coefficient in Zincblende Semiconductors," *IEEE J. Quantum Electron.* **30**, 256.

Fisher, R. A. (1983). *Optical Phase Conjugation.* Academic Press.

Fisher, M. A., Wiches, H., Kennedy, G. T., Grant, R. S., and Sibbett, W. (1993). "Ultrafast Nonlinear Refraction in an Active MQW Waveguide," *Electr. Lett.* **29**, 1185–1186.

Flytzanis, C. (1975). *Quantum Electronics,* (H. Rabin and C. L. Tang, eds.), Vol. I, Academic Press, p. 9.

Gibbs, H. M. (1985). *Optical Bistability: Controlling Light with Light,* Academic Press.

Grant, R. S. and Sibbett, W. (1991). "Observation of Ultrafast Nonlinear Refaction in InGaAsP Optical Amplifiers," *Appl. Phys. Lett.* **58**, 1119–1122.

Hagan, D. J., Van Stryland, E. W., Soileau, M. J., and Wu, Y. Y. (1988). "Self-Protecting Semiconductor Optical Limiters," *Opt. Lett.* **13**, 315.

Hall, K. L., Darwish, A. M., Ippen, E. P., Koren, U., and Raybon, G. (1993). "Femtosecond Index Nonlinearities in InGaAsP Optical Amplifiers," *Appl. Phys. Lett.* **62**, 1320–1323.

Hultgren, C. T. and Ipp0en, E. P. (1991). "Ultrafast Refractive Index Dynamics in AlGaAs Diode Laser Amplifiers," *Appl. Phys. Lett.* **59**, 635–638.

Hultgren, C. T. and Ippen, E. P. (1991). "Ultrafast Refractive Index Dynamics in AlGaAs Diode Laser Amplifiers," *Appl. Phys. Lett.* **59**, 635–638.

Hasselbeck, M. P., Said, A. A., Sheik-Bahae, M., and Van Stryland, E. W. (1993). "Nonlinear Optical Materials at $10\,\mu m$: From Picoseconds to Nanoseconds," *Proc. 1993 IRIS Specialty Group on Infrared Materials*, Bedford, MA.

Hasselbeck, M. P., Van Stryland, E. W., and Sheik-Bahae, M. (1997). "Dynamic Band Unblocking and Leakage Two-Photon Absorption in InSb," *Phys. Rev. B* **56**, 7395–7403.

Haug, H. (1988). *Optical Nonlinearities and Instabilities in Semiconductors*. Academic Press.

Hermann, J. A. and McDuff, R. G. (1993). "Analysis of Spatial Scanning with Thick Optically Nonlinear Media," *J. Opt. Soc. Am. B* **10**, 2056–2064.

Hermann, J. and Wilson, P. (1993). "Factors Affecting Optical Limiting and Scanning with Thin Nonlinear Samples," *Int. J. Nonlinear Opt. Phys.* **2**, 613–629.

Hill, J. R., Parry, G., and Miller, A. (1982). "Nonlinear Refractive Index Changes in CdHgTe at $175\,K$ with $10.6\,\mu m$ Radiation," *Opt. Commun.* **43**, 151.

Hong, M. Y., Chang, Y. H., Dienes, A., Heritage, J. P., and Delfyett, P. J. (1994). "Sub-picosecond Pulse Amplification in Semiconductor Laser Amplifiers: Theory and Experiment," *IEEE J. Quantum Electron.* **QE-30**, 1122–1131.

Hopfield, J. J., Worlock, J. M., and Park, K. (1963). "Two-Quantum Absorption Spectrum of KI," *Phys. Rev. Lett.* **11**, 414.

Hultgren, C. T., Dougherty, D. J., and Ippen, E. P. (1992). "Above- and Below-Band Femtosecond Nonlinearities in Active AlGaAs Waveguides," *Appl. Phys. Lett.* **61**, 2767–2769.

Hutchings, D. C. and Wherrett, B. S. (1994). "Theory of the Dispersion of Ultrafast Nonlinear Refraction in Zinc-Blende Semiconductors below the Band Edge," *Phys. Rev. B* **50**, 4622–4630.

Hutchings, D. C. and Wherrett, B. S. (1994b). "Polarization Dichroism of Nonlinear Refraction in Zinc-Blende Semiconductors," *Opt. Commun.* **111**, 507–512.

Hutchings, D. C. and Wherrett, B. S. (1995). "Theory of the Anisotropy of Ultrafast Nonlinear Refraction in Zincblende Semiconductors," *Phys. Rev. B* **52**, 8150–8159.

Hutchings, D. C., Sheik-Bahae, M., Hagan, D. J., Van Stryland, E. W. (1992). "Kramers-Kronig Dispersion Relations in Nonlinear Optics," *Opt. Quantum Electron.* **24**, 1–30.

Jain, R. K. and Klein, M. B. (1983). "Degenerate Four-Wave-Mixing in Semiconductors." In *Optical Phase Conjugation*, (R. A. Fisher, ed.), Academic Press, pp. 307–455.

Jones, H. D. and Reiss, H. R. (1977). "Intense-Field Effects in Solids," *Phys. Rev. B* **16**, 2466–2473.

Kaetner, F. X., Brovelli, L. R., Kopf, D., Kamp, M., Calasso, I. and Keller, U. (1995). "Control of Solid-State Laser Dynamics by Semiconductor Devices," *Opt. Eng.* **34**, 2024–2036.

Kajzar, F. and Messier, J. (1987). "Cubic Effects in Polydiacetylene Solutions and Thin Films." In *Nonlinear Optical Properties of Organic Molecules and Crystals*, Vol. 2, (D. S. Chemla and J. Zyss, eds.). Academic Press, Orlando, pp. 51–83.

Kane, E. O. (1957). "Band Structure of InSb," *J. Chem. Phys. Solids*, **1**, 249–261.

Kane, E. O. (1980). "Band Structure of Narrow Gap Semiconductors." In *Lecture Notes in Physics: Narrow Gap Semiconductors Physics and Applications*, (W. Zawadski, ed.), Vol. 133, Springer-Verlag, New York, pp. 13–31.

Kaplan, A. E. (1969). "External Self-Focusing of Light by a Nonlinear Layer," *Radiophys. Quantum Electron.* **12**, 692–696.

Keldysh, L. V. (1965). "Ionization in the Field of a Strong Electromagnetic Wave," *Sov. Phys. JETP* **20**, 1307–1314.

Keller, U., Weingarten, K. J., Kartner, F. X., Kopf, D., Braun, B., Jung, I. D., Fluck, R., Honninger, C., Matuschek, N., and Aus der Au, J. (1996). "Semiconductor Saturable Absorber Mirrors (SESAMs) for Femtosecond to Nanosecond Pulse Generation in Solid State Lasers," *IEEE J. Sel. Top. Quantum Electron.* **2**, 435–453.

Khurgin, J. B. (1994). "Nonlinear Response of the Semiconductor Quantum-Confined Structures Near and Below the Middle of the Gap," *J. Opt. Soc. B* **11**, 624–631.

Kogan, S. M. (1963). "On the Electromagnetics of Weakly Nonlinear Media," *Sov. Phys. JETP* **16**, 217.

LaGasse, M. J., Anderson, K. K., Wang, C. A., Haus, H. A., and Fujimoto, J. G. (1990). "Femtosecond Measurements of the Nonresonant Nonlinear Index in AlGaAs," *Appl. Phys. Lett.* **56**, 417–419.

Lee, S. G., McGinnis, B. P., Jin, R., Yumoto, J., Khitrova, G., Gibbs, H. M., and Peyghambarian, N. paper CtuC4, *CLEO '94 Technical Digest*, pp. 55.

Ma, H., Gomez, A. S. L., and de Araujo, C. B. (1991). "Measurement of a Nondegenerate Optical Nonlinearity Using a Two-Color Single Beam Method," *Appl. Phys. Lett.* **59**, 2666.

Maker, P., Terhune, R., and Savage, C. (1964). "Intensity-Dependent Changes in the Refractive Index of Liquids," *Phys. Rev. Lett.* **12**, 507.

Meystre, P. and Sargent, M. III, (1991). *Elements of Quantum Optics*, 2nd ed. Springer-Verlag.

Miller, A. and Duncan, D. (1987). "Optical Nonlinearities in Narrow Gap Semiconductors." In *Optical Properties of Narrow-Gap Low-Dimensional Structures*, (C. M. Sotomayer Torres, J. C. Portal, J. C. Mann, and R. A. Stradling, eds.), Plenum, New York.

Miller, D. A. B., Seaton, C. T., Prise, M. E., and Smith, S. D. (1981). "Band-Gap Resonant Nonlinear Refraction in III-V Semiconductors," *Phys. Rev. Lett.* **47**, 197.

Miller, A., Miller, D. A. B., and Smith, S. D. (1981). "Dynamic Non-Linear Optical Processes in Semiconductors," *Adv. Phys.* **30**, 697–800.

Mizrahi, V., DeLong, K. W., Stegeman, G. I., Saifi, M. A., and Andrejeco, M. J., (1989). "Two-Photon Absorption as a Limit to All-Optical Switching," *Opt. Lett.* **14**, 1140–1142.

Moran, M. J., She, C.-Y., and Carmen, R. L. (1975). "Interferometric Measurements of the Nonlinear Refractive Index Coefficient Relative to CS_2 in the Laser System Related Materials," *IEEE J. Quantum Electron.* **11**, 259.

Moss, T. S. (1980). "Theory of Intensity Dependence of Refractive Index," *Phys. Stat. Solidi B* **101**, 555–561.

Nussenzweig, H. M. (1972). *Causality and Dispersion Relations*, Academic Press, New York.

Owyoung, A. (1973). "Ellipse Rotation Studies in Laser Host Materials," *IEEE J. Quantum Electron.* **QE-9**, 1064.

Price, P. J. (1964). "Theory of Quadratic Response Functions," *Phys. Rev.* **130**, 1792.

Rader, T. R. and Gold, A. (1968). "Polarization Dependence of Two-Photon Absorption in Solids," *Phys. Rev.* **171**, 997–1003.

Ridener, F. L. Jr. and Good, R. H. Jr. (1975). "Dispersion Relations for Nonlinear Systems of Arbitrary Degree," *Phys. Rev. B* **11**, 2768.

Ross, I. N., Toner, W. T., Hooker, C. J., Barr, J. R. M., and Coffey, I. (1990). "Nonlinear Properties of Silica and Air for Picosecond Ultraviolet Pulses," *J. Mod. Opt.* **37**, 555–573.

Said, A. A., Sheik-Bahae, M., Hagan, D. J., Wei, T. H., Wang, J., Young, J., and Van Stryland, E. W. (1992). "Determination of Bound and Free-Carrier Nonlinearities in ZnSe, GaAs, CdTe, and ZnTe," *Opt. Soc. Am. B* **9**, 405–414.

Shank, C. V., Ippen, E. P., and Shapiro, S. L., eds. (1978). *Picosecond Phenomena.* Springer-Verlag, for example.

Sheik-Bahae, M. (1997). "Femtosecond Kerr-Lens Autocorrelation," *Opt. Lett.* **22**, 399–401.

Sheik-Bahae, M. and Ebrahimzadeh, M. (1997). "Measurements of Nonlinear Refraction in the Second-Order $\chi^{(2)}$ Materials $KTiOPO_4$, $KNbO_3$, β-BaB_2O_4, and LiB_3O_5," *Opt. Comun.* **142**, 294–298.

Sheik-Bahae, M., Hagan, D. J., and Van Stryland, E. W. (1990a). "Dispersion and Band-Gap Scaling of the Electronic Kerr Effect in Solids Associated with Two-Photon Absorption," *Phys. Rev. Lett.* **65**, 96–99.

Sheik-Bahae, M., Hutchings, D. C., Hagan, D. J., and Van Stryland, E. W. (1991). "Dispersion of Bound-Electronic Nonlinear Refraction in Solids," *IEEE J. Quantum Electron.* **QE-27**, 1296–1309.

Sheik-Bahae, M., Said, A. A., Hagan, D. J., Soileau, M. J., and Van Stryland, E. W. (1990). "Nonlinear Refraction and Optical Limiting in 'Thick' Media," *Opt. Eng.* **30**, 1228–1235.

Sheik-Bahae, M., Said, A. A., and Van Stryland, E. W. (1989). "High Sensitivity, Single Beam n_2 Measurements," *Opt. Lett.* **14**, 955–957.

Sheik-Bahae, M., Said, A. A., Wei, T. H., Hagan, D. J., and Van Stryland, E. W., (1990b). "Sensitive Measurements of Optical Nonlinearities Using a Single Beam," *IEEE J. Quantum Electron.* **QE-26**, 760–769.

Sheik-Bahae, M. and Van Stryland, E. W. (1994). "Ultrafast Nonlinearities in Semiconductor Laser Amplifiers," *Phys. Rev. B* **50**, 14171–14178.

Sheik-Bahae, M., Wang, J., Canto-Said, E. J., DeSalvo, R., Hagan, D. J., and Van Stryland, E. W. (1995). "Polarization Dependent Four-Wave Mixing and Two-Photon Coherence in Solids," *IEEE J. Quantum Electron.* **QE-31**, 1270–1273.

Sheik-Bahae, M., Wang, J., DeSalvo, J. R., Hagan, D. J., and Van Stryland, E. W. (1992). "Measurement of Nondegenerate Nonlinearities Using a 2-Color Z-Scan," *Opt. Lett.* **17**, 258–260.

Sheik-Bahae, M., Wang, J., and Van Stryland, E. W. (1994). "Nondegenerate Optical Kerr Effect in Semiconductors," *IEEE J. Quantum Electron.* **30**, 249–255.

Spence, D. E., Kean, P. N., and Sibbett, W. (1991). "60-fsec Pulse Generation From a Self-Mode-Locked Ti-Sapphire Laser," *Opt. Lett.* **19**, 4.

Stegeman, G. I., Kang, J. U., Aitchison, J. S., Ironside, C. N., and Villeneuve, A. (1996). "AlGaAs Waveguides Below Half the Bandgap: A Laboratory for Nonlinear Optics." In *Notions and Perspectives of Nonlinear Optics*, Nonlinear Optics Series, Vol. 3, (O. Keller, ed.). World Scientific, Singapore, pp. 428–457.

Stegeman, G. I. and Wright, E. M. (1990). "All Optical Waveguide Switching," *Opt. Quantum Electron* **22**, 95–122.

Sutherland, R., Pachter, R., Hood, P., Hagan, D., and Perry, J. eds. (1997). *Materials for Optical Limiting II*. Materials Research Society, Pittsburgh.

Tian, J.-G., Zang, W.-P., Zhang, C.-Z., and Zhang, G. (1995). "Analysis of Beam Propagation in Thick Nonlinear Media," *Appl. Opt.* **34**, 4331–4336.

Toll, J. S. (1956). "Causality and the Dispersion Relation: Logical Foundations," *Phys. Rev.* **104**, 1760.

Van Stryland, E. W. (1996). "Third-Order and Cascaded Nonlinearities." In *Laser Sources and Applications*, (A. Miller and D. M. Finlayson, eds.). IOP Publishing, Philadelphia, pp. 15–62.

Van Stryland, E. and Chase, L. (1994). "Two Photon Absorption: Inorganic Materials." In *Handbook of Laser Science and Technology*, Suppl. 2: "Optical Materials," (M. Weber, ed.). CRC Press, Section 8, pp. 299–328.

Van Stryland, E. W., Sheik-Bahae, M., Xia, T., Wamsley, C., Wang, Z., Said, A. A., and Hagan, D. J. (1994). "Z-Scan and EZ-Scan Measurements of Optical Nonlinearities," special issue of IJNOP on Novel Nonlinear Optical Polymers and Organic Materials, *Int. J. Nonlinear Opt. Phys.*, IJNOP, **3**(4), 489–500.

Van Stryland, E. W., Smirl, A. L., Boggess, T. F., Soileau, M. J., Wherrett, B. S., and Hopf, F. (1982). "Weak-Wave Retardation and Phase-Conjugate Self-Defocusing in Si." In *Picosecond Phenomena III*, (K. B. Eisenthal, R. M. Hochstrasser, W. Kaiser, and A. Laubereau, eds.), Springer-Verlag, p. 368.

Van Stryland, E. and Woodall, M. A. (1980). "Photoacoustic Measurement of Nonlinear Absorption in Solids." In *Laser-Induced Damage in Optical Materials*, NBS Special Publication 620, 50.

Van Stryland, E. W., Woodall, M. A., Vanherzeele, H., and Soileau, M. J. (1985). "Energy Band-Gap Dependence of Two-Photon Absorption," *Opt. Lett.* **10**, 490.

Van Stryland, E. W., Wu, Y. Y., Hagan, D. J., Soileau, M. J., and Mansour, K. (1988). "Optical Limiting with Semiconductors," *J. Opt. Soc. Am. B* **5**, 1980–1989.

Van Vechten, J. A. and Aspnes, D. E. (1969). "Franz-Keldysh Contribution to Third-Order Optical Susceptibilities," *Phys. Lett. A* **30**, 346.

Van Stryland, E. W., Vanherzeele, H., Woodall, M. A., Soileau, M. J., Smirl, A. L., Guha, S. and Boggess, T. F. (1985a). "Two-Photon Absorption, Nonlinear Refraction and Optical Limiting in Semiconductors," *Opt. Eng.* **24**, 613.

Volkov, D. M. (1935). "Concerning a Class of Solution of the Dirac Equation," *Z. Phys.* **94**, 250–260.

Wang, J., Sheik-Bahae, M., Said, A. A., Hagan, D. J., and Van Stryland, E. W. (1994). "Time-Resolved Z-Scan Measurements of Optical Nonlinearities," *J. Opt. Soc. Am. B* **11**, 1009–1017.

Weber, M. J., Milam, D., and Smith, W. L. (1978). "Nonlinear Refractive Index of Glasses and Crystals," *Opt. Eng.* **17**, 463.

Wherrett, B. S. (1984). "Scaling Rules for Multiphoton Interband Absorption in Semiconductors," *J. Opt. Soc. Am. B* **1**, 67–72.

Wherrett, B. S., Walker, A. C., and Tooley, F. A. P. (1988). "Nonlinear Refraction for cw Optical Bistability." In *Optical Nonlinearities and Instabilities in Semiconductors*, (H. Haug, ed.). Academic Press, New York, p. 239.

Williams, W. E., Soileau, M. J., and Van Stryland, E. (1984). "Optical Switching and n_2 Measurements in CS_2," *Opt. Commun.* **50**, 256.

Worlock, J. M. (1972). "Two-Photon Spectroscopy." In *Laser Handbook*, Vol. 2, (F. T. Arecchi and E. O. Schulz-Dubois, eds.), North-Holland, pp. 1223–1369.

Wu, T.-Y. and Ohmura, T. (1962). *Quantum Theory of Scattering*. Prentice Hall, Englewood Cliffs, New Jersey.

Xia, T., Hagan, D. J., Sheik-Bahae, M., and Van Stryland, E. W. (1994). "Eclipsing Z-Scan Measurement of $\lambda/10^4$ Wavefront Distortion," *Opt. Lett.* **19**, 317–319.

Xuan, M. P., Ferrier, J.-L., Gazengel, J., and Rivoire, G. (1984). "Picosecond Measurements of the Third-Order Susceptibility Tensor in Liquids," *Opt. Commun.* **51**, 433.